Structural basis of outer membrane protein insertion by the BAM complex

Yinghong Gu[1*], Huanyu Li[1*], Haohao Dong[1*], Yi Zeng[1*], Zhengyu Zhang[1*], Neil G. Paterson[2*], Phillip J. Stansfeld[3*], Zhongshan Wang[1,4,5], Yizheng Zhang[5], Wenjian Wang[6]#, Changjiang Dong[1]#

[1]Biomedical Research Centre, Norwich Medical School, University of East Anglia, Norwich Research Park, Norwich, NR4 7TJ, UK;

[2]Diamond Light Source, Harwell Science and Innovation Campus, Didcot, Oxfordshire, OX11 0DE, UK;

[3]Department of Biochemistry, University of Oxford, South Parks Road, Oxford OX1 3QU, UK;

[4]Jiangsu Province Key Laboratory of Anesthesiology, Xuzhou Medical College, Xuzhou 221004, China

[5]Key Laboratory of Bio-resources and Eco-environment, Ministry of Education, Sichuan Key Laboratory of Molecular Biology and Biotechnology, College of Life Sciences, Sichuan University, Chengdu, 610064, China

[6]Laboratory of Department of Surgery, the First Affiliated Hospital, Sun Yat-sen University, 58 Zhongshan Road II, Guangzhou, Guangdong, 510080, China.

*These authors contributed equally to this work

#To whom correspondence should be addressed, C.Dong@uea.ac.uk or w166w2000@aliyun.com

All Gram-negative bacteria, mitochondria and chloroplasts have outer membrane proteins (OMPs), which perform many fundamental biological processes. The OMPs in Gram-negative bacteria are inserted and folded into the outer membrane (OM) by the β-barrel assembly machinery (BAM). The mechanism involved is poorly understood due to the absence of a structure of the entire BAM complex. Here we report two crystal structures of the *E. coli* BAM complex in two distinct states: an inward-open and a lateral-open state. Our structures reveal that the five polypeptide transport-associated domains of BamA form a ring architecture with four associated lipoproteins, BamB-E in the periplasm. Our structural, functional studies and molecular dynamics simulations indicate that these subunits rotate with respect to the integral membrane β-barrel of BamA to induce movement of the β-strands and promote insertion of the nascent OMP.

Outer membrane proteins (OMPs) play important roles in Gram-negative bacteria, mitochondria and chloroplasts in nutrition transport, protein import, secretion, and other fundamental biological processes[1-3]. Dysfunction of mitochondria outer membrane proteins are linked to disorders such as diabetes, Parkinsons and other neurodegenerative diseases[4,5]. The OMPs are inserted and folded correctly into the outer membrane (OM) by the conserved OMP85 family proteins[6-8], suggesting that similar insertion mechanisms may be used in Gram-negative bacteria, mitochondria and chloroplasts.

In Gram-negative bacteria, OMPs are synthesized in the cytoplasm, and are transported across the inner membrane by SecYEG into the periplasm[8,9]. The seventeen kilodalton (kDa) protein (Skp) and the survival factor A (SurA) chaperones escort the unfolded OMPs across the periplasm to the β-barrel assembly machinery (BAM), which is responsible for insertion and assembly of OMPs into the OM[10-12]. In *Escherichia coli*, the BAM complex consists of BamA and four lipoprotein subunits, BamB, BamC, BamD and BamE. BamA is comprised of five N-terminal polypeptide transport-associated (POTRA) domains and a C-terminal OMP transmembrane barrel, while the four lipoproteins are affixed to the membrane by N-terminal lipid-modified cysteines. Of these subunits, BamA and BamD are essential[3,6]. One copy of each of these five proteins is required to form the BAM complex with an approximate molecular weight of 200 kDa (Extended Data Fig. 1). *In vitro* reconstitution of the *E. coli* BAM complex and functional assays showed that all five subunits are required to obtain the maximum activity of BAM[13-16]. Individual structures of BamA[17-20], BamB[21-25], BamC[22,26], BamD[22,27,28] and BamE[22,29,30] have previously been reported, as have complex structures of BamD with the N-terminal domain of BamC[31], and BamB with POTRA 3 and 4 of BamA[32]. Nonetheless, the precise mechanism of OMP

insertion by the BAM complex is largely hampered by the lack of a complete structure of the BAM complex[11,32]. Furthermore it is unknown how BAM manages to insert OMPs into the OM without the use of ATP, proton motive forces or redox potentials[33,34].

Here we report two novel crystal structures of the *E. coli* BAM complex: BamABCDE and BamACDE. The complexes reveal a unique ring architecture that adopts two distinct conformations: an inward-open and a novel lateral-open. Furthermore, comparison of the two complexes reveals that the periplasmic units are rotated with respect to the barrel, which appears to be linked to significant conformational changes in the β-strands β1C-β6C of the barrel. Taken together this suggests a novel insertion mechanism whereby rotation of the BAM periplasmic ring promotes insertion of OMPs into the OM. To our knowledge, this is the first reported crystal structure of an intramembrane barrel with a lateral-open conformation.

Unique architecture of two *E. coli* BAM complexes

X-ray diffraction data of selenomethionine labelled crystals were collected to 3.9 Ångström (Å) resolution and the BAM structure was determined by single-wavelength anomalous dispersion (SAD) and manual molecular replacement (Methods, Extended Data Table 1). The first structure contained four proteins: BamA, BamC, BamD and BamE (Fig. 1a-c), with the electron density and crystal packing indicating that the BamB is absent in the complex. This was confirmed by SDS-PAGE analysis of the crystals (Extended Data Fig. 1 and Supplementary Data Fig. S1). In this model, BamA, BamC, BamD and BamE contain residues E22-I806, C25-K344, E26-S243, and C20-E110, respectively. The machinery is approximately 115 Å in length, 84 Å in width and 132 Å in height (Fig. 1a).

The architecture of BamACDE resembles a top hat with an opening in the crown. This crown is formed by the BamA β-barrel with the encircling POTRA domains and associated proteins forming the brim. The C-terminal β-barrel of BamA projects out of the complex and is fully immersed in the OM while the five POTRA domains of BamA and the BamD form a ring in the periplasm (Fig. 1a-c). The other subunits of the complex surround this central BamAD core. The coiled N-terminal loop of BamC is bound to BamD, as is its N-terminal globular domain, which also interacts with POTRA 1 of BamA. The C-terminal globular domain of BamC interacts with BamD and POTRA 2. Interestingly, for one of the two BamACDE complexes in the asymmetric unit cell no electron density was observed for the N-terminal and C-terminal globular domains of BamC, which may indicate inherent flexibility (Extended Data Fig. 2). This flexibility was also observed in the MD simulations. Finally, BamE is found at the opposite end of the complex, coupling the C-terminal domain of BamD to POTRA 4 and 5 of BamA, adjacent to the barrel (Fig. 1b, c).

In order to obtain a structure of the complex with all five subunits, we increased the expression level of BamB (Methods). The structure of BamABCDE was determined by co-crystallization with sodium iodine and SAD and manual molecular replacement techniques to a resolution of 2.9 Å (Methods, Extended Data Table 1). The structure we describe below is based on this BamABCDE complex unless otherwise mentioned. The β-strands of BamA's C-terminal barrel are named as β1C-β16C for consistency with previous reports. The top hat architecture of BamABCDE is similar to that of BamACDE with dimensions of around 120 Å in length, 98 Å in width and 140 Å in height, with the periplasmic ring structure retained (Fig. 1d-f). In the BamABCDE structure, the opening in the crown of the top hat is now closed. This model of the BAM complex contains BamB (residues K31-T391), which is shown to

bind to POTRA 2 and 3. Although SDS-PAGE analysis of the crystals showed BamC is intact in the BamABCDE crystals (Extended Data Fig. 1), electron density is only visible for the N-terminal loop (residues V35 to P88), bound to BamD. This indicates that the rest of BamC is highly flexible. Molecular dynamics (MD) simulations of the BamABCDE and BamACDE complexes suggests that both complexes are otherwise stable and the periplasmic ring structure remains intact during the simulations (Extended Data Fig. 3, Supplementary Data Video S1 and Supplementary Data Fig. S2, 3 and 4).

Inward- and lateral-open conformations

In the structure of the BamABCDE complex, the extracellular loops (L-1 to L-8) cap the pore of BamA to completely close it to the extracellular side, while the periplasmic mouth is fully open to the periplasm (Fig. 2a, b). This conformation is similar to all reported barrel structures of BamA, however, the POTRA domains are significantly different (Extended Data Fig. 4). The POTRA domains of BamABCDE appear locked through their interactions with BamD, which together form a ring apparatus that may feed the unfolded OMP into the assembly machinery. It is worth noting that the β16C of both *Neisseria gonorrhoeae* BamA and the BamABCDE complex coils toward the inside of the barrel lumen, creating a gap between β1C and β15C of the barrels (Fig. 1d, Fig. 2f and Extended Data Fig. 4), which may provide a path for insertion of the OMPs.

In contrast, in the structure of BamACDE, extracellular loops L-1, L-2 and L-3 are displaced from the pore, opening the barrel laterally between β1C and β16C. This exposes the barrel lumen to both the extracellular leaflet of the OM and the outside of the cell (Fig. 2c, d). Conversely, on the periplasmic side, POTRA 5 and turn T-1 to T-

4 completely plug the barrel (Fig. 2d and Extended Data Fig. 5). The barrel of BamA in the BamACDE structure is therefore in a lateral-open conformation. The first 6 β-strands, β1C to β6C, perform a scissor-like movement to rotate away from the pore to a maximum angle of around 65° and distance of about 15 Å (Fig. 2e and Extended Data Fig. 5). The other strands of the barrel remain unchanged. These conformational changes open the barrel laterally to the OM and the extracellular side, and, in conjunction with POTRA 5, close the periplasmic mouth (Fig. 2c, d and Extended Data Fig. 5). Such a mechanism of conformational changes between inward- and outward-open conformations to transport small molecular substrates is common for α-helical inner membrane protein transporters[35]. However, to our knowledge, this is the first crystal structure report to date of a β-barrel that may alternate between both inward- and lateral-open conformations. The novel architecture of the lateral-open conformation is likely to facilitate the insertion of β-strands of the OMP into the OM, while permitting the interlinking extracellular loops to extend out of the cell upon insertion.

It was suggested that lateral separation between β1C and β16C is required for normal BamA function by disulfide bond cross-linking[36]. To test the two solved conformations, *in vivo* cross-links were designed to interlock BamA in one of the two conformational states. Two double cysteine mutations, E435C/S658C and E435C/S665C, were created to capture BamA in the inward-open conformation (Fig. 2f), and one double mutation, G393C/G584C, was produced to restrain BamA in the lateral-open conformation (Fig. 2g). The single cysteine mutations do not affect cell growth, while the double cysteine mutations G393C/G584C, E435C/S665C and E435C/S658C are all lethal (Fig. 2h, i). In addition, the double cysteine mutants are folded into the OM and can be rescued by the addition of 2 mM reducing reagent

Tris(2-carboxyethyl)phosphine hydrochloride (TCEP) (Fig. 2j, k, Extended Data Fig. 5 and Supplementary Data Fig. S5), which breaks the disulfide bonds and therefore unlocks the structure, providing strong evidence that the barrel can exist in the two resolved conformations in the bacterial OM.

Essential interactions between BamA and BamD

Previous mutagenesis analysis has suggested that only POTRA 5 of BamA associates with BamD[37], however prior to this study no structures of this complex have been solved. In our structures 12 residues of BamD interact with 17 residues of POTRA 5 (Fig. 3a, Extended Data Fig. 6 and Supplementary Data Table 1). In addition to contacts with POTRA 5, our structures reveal that BamD also interacts with V480 and D481 of periplasmic turn T-2 of the BamA barrel and also forms contacts with POTRA 1 and 2. These interactions complete the ring structure (Extended Data Fig. 7 and Supplementary Data Table 1).

MD simulations of only the core BamAD periplasmic ring from both structures retains the cyclic complex. Removal of BamD markedly increases the dynamics of POTRA 1 and 2 in the BamACDE conformation (Extended Data Fig. 3, Supplementary Data Video S1). In this instance, the POTRA domains rotate in a counter-clockwise direction towards the OM. This rotation also causes POTRA 3 to separate from the T-5 and T-6 periplasmic turns of the BamA barrel (Extended Data Fig. 3 and Supplementary Data Video S1). In contrast, simulations of only BamA from the BamABCDE structure, results in POTRA 2 coupling to POTRA 5, thereby stabilizing POTRA 1 and 2. However, to achieve this configuration, POTRA 3 and 4 separate from the barrel, with a degree of deformation to POTRA 3, suggesting that this is a strained conformation.

To test whether the BamA and BamD interactions are required for BAM function, BamA POTRA 5 mutants E373K and R366E were generated. Functional assays showed that R366E severely impairs cell growth, while E373K is lethal to the *E. coli* cells (Extended Data Fig. 7). In the structures, BamA E373 and BamD R197 form a salt-bridge (Fig. 3a). An R197L BamD mutation was able to rescue BamA E373K[37].

BamB regulates BamA conformation

The most apparent differences between the two solved structures are the presence of BamB in the BamABCDE complex, while BamC is more clearly resolved in the BamACDE complex (Fig. 2a, c). In addition, the POTRA domains of BamA are found in two distinct conformations, with a larger separation observed between POTRA 3 and 5 in the BamACDE complex. Speculatively, this could be due to the absence of BamB, which binds to POTRA 2 and 3 in the BamABCDE complex and is known to have a regulatory role[3,22,23]. The overall interface between BamA and BamB is around 1080 $Å^2$, and is comprised of the three β-strands of POTRA 3 and a loop consisting of residues T245-K251 that anchors to the center of the BamB β-propeller (Fig. 3b, Extended Data Fig. 7 and Supplementary Data Table 2). The BamB loops at the BamA binding side adopt conformational changes to bind to POTRA 3[21,22] (Extended Data Fig. 7), consistent with the BamB structure in complex with POTRA 3 and 4[32]. BamB also interacts with residues K135 and Y147 of POTRA 2 (Fig. 3b). As a result, the binding of BamB appears to induce local conformational changes in POTRA 2 and 3 with a root-mean-square deviation (RMSD) of 3.57 Å over 159 Cα atoms (Extended Data Fig. 7).

Both periplasmic turns T-5 and T-6 of the BamA barrel are more ordered in the BamABCDE structure and interact with POTRA 3 (Extended Data Fig. 6). In the

BamACDE complex POTRA 3 separates from the periplasmic turns (Fig. 2c), indicating that BamB may play a role in controlling the structural rearrangements of the barrel through POTRA 3. It is worth noting that POTRA 5 also has extensive contacts with the periplasmic turns T-1, T-2 and T-3 of the barrel domain in the BamABCDE structure (Extended Data Fig. 6), and we speculate that the conformational changes of POTRA domains may play a role in controlling the barrel's conformations.

In the MD simulations, the tight coupling between POTRA 3 and BamB was retained. However, in the absence of BamB, the simulations reveal greater dynamics of POTRA 3 and 4, with both domains moving away from the barrel and the membrane (Supplementary Data Video S1). This suggests that BamB is important for coupling of POTRA 3 at the appropriate height with respect to the barrel and OM.

BamE and BamC interactions with BamA and BamD

Previous studies suggested that BamE only binds to BamD directly [38,39]. Surprisingly, both BamABCDE and BamACDE structures show that BamE is not only positioned between BamA and BamD, but also forms contacts with BamC (Fig. 4a, Extended Data Fig. 6, 8 and Supplementary Data Table 3, 4). Interestingly, the BamE residues P67 and F68 also interact with BamC residues M56 and I57 (Extended Data Fig. 8), suggesting that BamC, BamD and BamE form a network to regulate the conformations of BamA.

BamE residues I32, Q34, L63 and R78 interact with both BamA and BamD. Mutations to any of these residues caused defects to the OM[29]. Additionally, single BamE mutations N36 and Y37 at the BamE and BamA interface or residues M64,

D66, F74, V76, Q88 at BamE and BamD interface caused defects of the OM[29]. These data suggest that BamE plays an important role in OMP assembly.

The whole BamC structure is revealed in the BamACDE complex. BamC forms extensive contacts with BamD, with the average interface of 2686 Å^2 (Fig. 4b, Extended Data Fig. 8 and Supplementary Data Table 5). The N-terminal loop of BamC, up to residue G94, is largely unstructured, coiling round BamD and forming a cluster of contacts with BamE. The N-terminal globular domain of BamC interacts with the N-terminal domain of BamD and POTRA 1 of BamA (Extended Data Fig. 8). The C-terminal globular domain interacts principally with POTRA 2, via their β-sheets (Fig. 4b).

The C-terminal globular domain of BamC binds to POTRA 2 in one of the BamACDE complexes. This likely enhances the periplasmic ring structure formed by BamA and BamD, and plays a role in the conformational changes of BAM. Comparison of the two BamACDE complexes in the asymmetric unit reveals differences in the barrel domain, with an RMSD of 0.91 Å over 378 Cα atoms, while the periplasmic ring is somewhat rotated, with respect to the barrel (Extended Data Fig. 2). SDS-PAGE analysis confirmed that both BamACDE and BamABCDE crystals contain full length BamC (Extended Data Fig. 1), suggesting that the two globular domains of BamC are dynamic. MD simulations, with the addition of the BamC globular domains to this structure, also show that these domains are not tightly coupled to the complex. Indeed, in the simulations of both complexes BamC shows the least stability of all five subunits. The total interface between BamC with BamA is around 794 Å^2 in the BamACDE structure (Fig. 4b, Extended Data Fig. 8 and Supplementary Data Table 6). The MD simulations of BamACDE complex without BamC suggest that the POTRA 1 moves toward to the membrane, while POTRA 3

moves toward the barrel and engages with the periplasmic turns T-5 and T-6 (Extended Data Fig. 3). In the simulations of the inward-open BamABCDE complex the absence of BamC globular domains has limited effects on the overall structure, as BamD is more tightly coupled to the POTRA domains. Taken together, all four lipoproteins BamB, C, D and E have direct contacts with BamA POTRA domains, which may be important in terms of conformation and functional regulation. Analysis of the BAM subunits reveal that conserved residues are mapped to those regions involved in inter-subunit protein-protein interactions (Extended Data Fig. 9 and Supplementary Data Fig. S6).

All the POTRA domains of BamA have the βααββ fold[17]. An NMR study suggested that the β-sheet of the POTRA domains may bind substrate in a non-specific manner[40]. Our structural studies show that both BamB and the C-terminal domain of BamC bind to the POTRA domains 2 and 3 through their β-sheets. The three β-strands of POTRA 5 adopt a significant conformational change, from 126° between the β1C and the POTRA 5 β-sheet (β3) in the inward-open state to 165° in the lateral-open state, aligning the β-sheet of POTRA 5 with β1C. Additionally, almost all BamA of Gram-negative bacteria, SAM50 of mitochondria and OEP80 of chloroplasts have the last POTRA domain, indicating that the POTRA 5 of BamA may play an important role in the insertion of OMPs. To test this possibility, single proline substitutions (K351P, R353P, T397P, D399P, D401P, V415P, K417P, K419P), double proline substitutions (K351P/R353P, T397P/D399P, D399P/D401P, T397P/D401P, V415P/K417P, K417P/K419P, V415P/K419P) and triple proline substitution (T397P/D399P/D401P) were generated in β1, β2, and β3 of BamA POTRA 5. Functional assays showed that all single mutants (except K351P) and double mutants at β-strand 2 (T397P/D399D, D399P/D401P, T397P/D401P) did not

affect *E. coli* cell growth, but single substitution K351P at the β-strand 1, double proline substitutions at the β-strand 1 (K351P/R353P) and the β-strand 3 (V415P/K417P, or K417P/K419P, or V415P/K419P) are lethal, and triple mutation at β-strand 2 (T397P/D399P/D401P) impaired the cell growth (Fig. 5a, b). This strongly suggests that the β-sheet, especially the β-strands 1 and 3 of POTRA 5, may play a critical role in OMPs insertion, possibly by β-augmentation of the unfolded OMPs.

Mechanism and conclusion

In Gram-negative bacteria, outer membrane barrel proteins are inserted and assembled into the OM by the BAM complex. Our studies have revealed the three-dimensional architecture of the entire *E. coli* BAM complex, trapped in two distinct conformational states. The structures suggest that a rotation of the periplasmic ring (Extended Data Fig. 2, 5, Supplementary Data Video S1, 2) and conformational changes of the POTRA domains and BamB-E (Extended Data Fig. 10) induces the significant conformational changes to the barrel of BamA required for BAM-induced OMP insertion (Fig. 2e). Considering all four lipoproteins subunits, BamB-E, directly interact with POTRA domains, the ring architecture of the *E. coli* BAM complex may be an efficient way to coordinate all BAM subunits and thereby promote OMPs insertion into the OM. (Extended Data Fig. 10 and Supplementary Data Video 2).

To accomplish insertion, the OM periplasmic lipid head groups must be circumnavigated by the unfolded or partially-folded OMPs[41]. A number of mechanisms for OMP insertion have previously been described[18,36], with the "BamA-assisted model" and "the budding model" currently the two most favoured[36].

Our structures reveal a 30° rotation of the periplasmic ring complex, which interacts directly with the lipid headgroups of the OM (Extended Data Fig. 5, 10). This rotation

is likely coupled to the 65° tilting of strands β1C-6C of the BamA barrel and the partial separation of the lateral gate, formed by β1C and β16C (Fig. 2c, e). This exposes the barrel lumen to the core of the OM, whilst also inducing a degree of membrane instability to facilitate OMP insertion. The BamA homologue, SAM50, in mitochondria will likely use a similar scissor-like movement of the barrel strands to promote OMPs insertion into the mitochondrial OM; however, this is performed in absence of the periplasmic ring.

In summary, our structural, functional and molecular dynamics simulations have revealed that the BAM complex has a unique ring architecture and is able to adopt both inward-open and a lateral-open states. We hypothesize that these structures represent the resting (BamABCDE) and post-insertion (BamACDE) states of the complex. These findings shed an important light on how the BAM subunits work together to insert unfolded OMPs into the OM without using ATP and sets up an important platform for further studies of OM biogenesis and the potential development of novel therapies, e.g. by inhibiting complex formation.

References

1 Walther, D. M., Rapaport, D. & Tommassen, J. Biogenesis of β-barrel membrane proteins in bacteria and eukaryotes: evolutionary conservation and divergence. *Cell. Mol. Life Sci.* **66**, 2789-2804 (2009).

2 Tommassen, J. Assembly of outer-membrane proteins in bacteria and mitochondria. *Microbiology* **156**, 2587-2596 (2010).

3 Wu, T. *et al*. Identification of a multicomponent complex required for outer membrane biogenesis in *Escherichia coli*. *Cell* **121**, 235-245 (2005).

4. Sasaki K, *et al*. VDAC: Old protein with new roles in diabetes. *Am. J. Physiol. Cell Physiol.* **303**, C1055–C1060 (2012).

5. Bender A, *et al*. TOM40 mediates mitochondrial dysfunction induced by α-synuclein accumulation in Parkinson's disease. *PLoS One* **8**, e62277 (2013).

6 Knowles, T. J., Scott-Tucker, A., Overduin, M. & Henderson, I. R. Membrane protein architects: the role of the BAM complex in outer membrane protein assembly. *Nat. Rev. Microbiol.* **7**, 206-214 (2009).

7 Hagan, C. L., Silhavy, T. J. & Kahne, D. β-barrel membrane protein assembly by the Bam complex. *Annu. Rev. Biochem.* **80**, 189-210 (2011).

8 Ricci, D. P. & Silhavy, T. J. The Bam machine: a molecular cooper. *Biochim. Biophys. Acta* **1818**, 1067-1084 (2012).

9 Rigel, N. W. & Silhavy, T. J. Making a beta-barrel: assembly of outer membrane proteins in Gram-negative bacteria. *Curr. Opin. Microbiol.* **15**, 189-193 (2012).

10 Webb, C. T., Heinz, E. & Lithgow, T. Evolution of the β-barrel assembly machinery. *Trends. Microbiol.* **20**, 612-620 (2012).

11 Noinaj, N., Rollauer, S. E. & Buchanan, S. K. The β-barrel membrane protein insertase machinery from Gram-negative bacteria. *Curr. Opin. Struct. Biol.* **31**, 35-42 (2015).

12 Misra, R., Stikeleather, R. & Gabriele, R. *In vivo* roles of BamA, BamB and BamD in the biogenesis of BamA, a core protein of the β-barrel assembly machine of *Escherichia coli*. *J. Mol. Biol.* **427**, 1061-1074 (2015).

13 McMorran, L. M., Brockwell, D. J. & Radford, S. E. Mechanistic studies of the biogenesis and folding of outer membrane proteins *in vitro* and *in vivo*: what have we learned to date? *Arch. Biochem. Biophys.* **564**, 265-280 (2014).

14 Hagan, C. L., Kim, S. & Kahne, D. Reconstitution of outer membrane protein assembly from purified components. *Science* **328**, 890-892 (2010).

15 Hagan, C. L., Westwood, D. B. & Kahne, D. Bam lipoproteins assemble BamA *in vitro*. *Biochemistry* **52**, 6108-6113 (2013).

16 Roman-Hernandez, G., Peterson, J. H. & Bernstein, H. D. Reconstitution of bacterial autotransporter assembly using purified components. *Elife* **3**, e04234 (2014).

17 Kim, S. *et al*. Structure and function of an essential component of the outer membrane protein assembly machine. *Science* **317**, 961-964 (2007).

18 Noinaj, N. *et al*. Structural insight into the biogenesis of β-barrel membrane proteins. *Nature* **501**, 385-390 (2013).

19 Ni, D. *et al*. Structural and functional analysis of the β-barrel domain of BamA from *Escherichia coli*. *FASEB J.* **28**, 2677-2685 (2014).

20 Albrecht, R. *et al*. Structure of BamA, an essential factor in outer membrane protein biogenesis. A*cta Crystallogr. D Biol. Crystallogr.* **70**, 1779-1789 (2014).

21 Noinaj, N., Fairman, J. W. & Buchanan, S. K. The crystal structure of BamB suggests interactions with BamA and its role within the BAM complex. *J. Mol. Biol.* **407**, 248-260 (2011).

22 Albrecht, R. & Zeth, K. Structural basis of outer membrane protein biogenesis in bacteria. *J. Biol. Chem.* **286**, 27792-27803 (2011).

23 Dong, C., Yang, X., Hou, H. F., Shen, Y. Q. & Dong, Y. H. Structure of *Escherichia coli* BamB and its interaction with POTRA of BamA. *Acta Crystallogr. D Biol. Crystallogr.* **68**, 1134-1139 (2012).

24 Kim, K. H. & Paetzel, M. Crystal structure of *Escherichia coli* BamB, a lipoprotein component of the beta-barrel assembly machinery complex. *J. Mol. Biol.* **406**, 667-678 (2011).

25 Heuck, A., Schleiffer, A. & Clausen, T. Augmenting β-augmentation: structural basis of how BamB binds BamA and may support folding of outer membrane proteins. *J. Mol. Biol.* **406**, 659-666 (2011).

26 Warner, L. R. *et al*. Structure of the BamC two-domain protein obtained by Rosetta with a limited NMR data set. *J. Mol. Biol.* **411**, 83-95 (2011).

27 Sandoval, C. M., Baker, S. L., Jansen, K., Metzner, S. I. & Sousa, M. C. Crystal structure of BamD: an essential component of the β-barrel assembly machinery of gram-negative bacteria. *J. Mol. Biol.* **409**, 348-357 (2011).

28 Dong, C., Hou, H. F., Yang, X., Shen, Y. Q. & Dong, Y. H. Structure of Escherichia coli BamD and its functional implications in outer membrane protein assembly. *Acta Crystallogr. D Biol. Crystallogr.* **68**, 95-101 (2012).

29 Knowles, T. J. *et al*. Structure and function of BamE within the outer membrane and the β-barrel assembly machine. *EMBO Rep.* **12**, 123-128 (2011).

30 Kim, K. H. *et al*. Structural characterization of *Escherichia coli* BamE, a lipoprotein component of the β-barrel assembly machinery complex. *Biochemistry* **50**, 1081-1090 (2011).

31 Kim, K. H., Aulakh, S. & Paetzel, M. Crystal structure of β-barrel assembly machinery BamCD protein complex. *J. Biol. Chem.* **286**, 39116-39121 (2011).

32 Jansen, K. B., Baker, S. L. & Sousa, M. C. Crystal structure of BamB bound to a periplasmic domain fragment of BamA, the central component of the β-barrel assembly machine. *J. Biol. Chem.* **290**, 2126-2136 (2015).

33 Hagan, C. L. & Kahne, D. The reconstituted *Escherichia coli* Bam complex catalyzes multiple rounds of β-barrel assembly. *Biochemistry* **50**, 7444-7446 (2011).

34 Rigel, N. W., Ricci, D. P. & Silhavy, T. J. Conformation-specific labeling of BamA and suppressor analysis suggest a cyclic mechanism for β-barrel assembly in *Escherichia coli*. *Proc. Natl Acad. Sci. USA* **110**, 5151-5156 (2013).

35 Noinaj, N. & Buchanan, S. K. Structural insights into the transport of small molecules across membranes. *Curr. Opin. Struc. Biol.* **27**, 8-15 (2014).

36 Noinaj, N., Kuszak, A. J., Balusek, C., Gumbart, J. C. & Buchanan, S. K. Lateral opening and exit pore formation are required for BamA function. *Structure* **22**, 1055-1062 (2014).

37 Ricci, D. P., Hagan, C. L., Kahne, D. & Silhavy, T. J. Activation of the *Escherichia coli* β-barrel assembly machine (Bam) is required for essential components to interact properly with substrate. *Proc. Natl Acad. Sci. USA* **109**, 3487-3491 (2012).

38 Rigel, N. W., Schwalm, J., Ricci, D. P. & Silhavy, T. J. BamE modulates the *Escherichia coli* beta-barrel assembly machine component BamA. *J. Bacteriol.* **194**, 1002-1008 (2012).

39 Tellez, R., Jr. & Misra, R. Substitutions in the BamA β-barrel domain overcome the conditional lethal phenotype of a ΔbamB ΔbamE strain of *Escherichia coli*. *J. Bacteriol.* **194**, 317-324 (2012).

40 Bennion, D., Charlson, E. S., Coon, E. & Misra, R. Dissection of β-barrel outer membrane protein assembly pathways through characterizing BamA POTRA 1 mutants of *Escherichia coli*. *Mol. Microbiol*. **77**, 1153-1171 (2010).

41 Gessmann, D. *et al*. Outer membrane β-barrel protein folding is physically controlled by periplasmic lipid head groups and BamA. *Proc. Natl Acad. Sci. USA* **111**, 5878-5883 (2014).

Supplementary Information is linked to the online version of the paper at www.nature.com/nature.

Acknowledgements

We thank Dr. Harris D Bernstein for providing HDB150 strain and plasmid pJH114 and Prof. Thomas J. Silhavy for providing JCM166 cells. We appreciate the staff at I24, I02 and I03 of Diamond Light Source UK for beamtime (proposal mx9475) and their assistance with data collection. CJD is a recipient of the Wellcome Trust investigator award (WT106121MA) and supported by Medical Research Council (G1100110/1). WJW thanks for the support of Science and technology program of Guangzhou, China (201510010040) and China National Natural Science Foundation of Guangdong (2015A030313152).

Author Contributions

CJD, WJW and YHG conceived and designed the experiments. CJD and WJW supervised the project. YHG, YZ, ZSW and YZZ designed primers and generated the constructs for protein expression and functional assays. YHG, YZ, HD, HYL, ZYZ and ZSW expressed, purified and crystallized the BamABCDE and BamACDE complexes. YHG and YZ optimized crystallization, harvested crystals and performed site-directed mutagenesis, functional assays, heat-modifiability assays and western blot. CJD, NP, YHG and WJW undertook data collection and structure determination.

NP and CJD did the structure refinements. PJS performed the molecular dynamics simulations. YHG, CJD, PJS and NP prepared tables and figures. CJD, YHG, WJW, PJS and NP wrote and revised the manuscript.

Author Information

The atomic coordinates and structure factors of BamABCDE and BamACDE are deposited at the Protein Data Bank under access code 5D0O and 5D0Q. Reprints and permissions information is available at www.nature.com/reprints. The authors declare no financial competing interests. Correspondence and requests for materials should be addressed to CJD (c.dong@uea.ac.uk) or WJW (w166w2000@aliyun.com).

Figure legends

Figure 1 | Structure of two complexes of *E. coli* β-barrel assembly machinery. Two structures of *E. coli* BAM: BamABCDE and BamACDE. The BamA (red) C-terminal barrel is embedded in the OM, while the N-terminal domain of BamA is in the periplasm, forming a novel circular structure with lipoproteins BamB (green), BamC (blue), BamD (magenta) and BamE (cyan). **a**, **b** and **c**, Cartoon representation of the structure of BamACDE complex, viewed for the membrane plane, extracellular and periplasm, respectively. BamD interacts with POTRA 1, 2 and 5 to form a ring structure in the periplasm, while BamC binds to both BamD and POTRA 1 and 2 of BamA. BamE forms contacts with both BamA and BamD. The dimensions of BamACDE were measured at the widest points of the outer surfaces of the complex. **d**, **e** and **f**, Cartoon representation of BamABCDE structure, viewed from the membrane plane, extracellular and periplasm, respectively. BamB interacts with

POTRA 2 and 3, while only N-terminal loop of BamC forms contacts with BamD. The dimensions of BamABCDE were measured as in **a**.

Figure 2 | Inward- and lateral-open conformations of BAM. BamA-E are in the same colors as in Figure 1. **a**, Membrane view of the molecular surface of BamABCDE. The pore of BamA is completely sealed at the extracellular side by the extracellular loops. **b**. Periplasmic view of BamABCDE. The barrel is open to the periplasm (indicated by the arrow). **c**, Membrane view of the molecular surface of BamACDE. The barrel is open laterally to the OM and the extracellular side (indicated by the arrow). **d**, Periplasmic view of BamACDE surface structure. The barrel is completely closed to the periplasm. **e**, The significant conformational changes of the BamA barrel domain between the inward-open (red) and the lateral-open (yellow) conformations. The barrel strands β1C-β6C of BamA have been rotated about 65° with the distance around 15 Å to laterally open the barrel from the inward-open state. **f**, The double mutation E435C/S665C or E435C/S658C is expected to lock the barrel in the inward-open conformation. Residues I806-K808 of the β16C of BamA coils toward the inside of the barrel lumen. **g**, The G393C/G584C mutant is expected to lock the barrel in the lateral-open conformation. **h**, The functional assays of the mutants. The single residue mutations do not affect the *E. coli* cell growth, but the double cysteine mutations kill the bacteria. 1, 2, 3, 4, 5, 6, 7, 8, 9, and 10 represent the wild type BamA, the vector without BamA, BamA mutants G393C, G584C, G393C/G584C, E435C, S665C, S658C, E435C/S665C and E435C/S658C, respectively. **i**, The protein expression levels of BamA mutants in the OM were checked by western blotting. **j**, The reducing reagent TCEP could rescue the double cysteine mutations at 2 mM. **k**, The protein expression levels of BamA double

cysteine mutants in absence and in present of TCEP were checked by western blotting.

Figure 3 | BamA interacts with BamD and BamB in BamABCDE complex. BamD contacts POTRA domains 1, 2 and 5 to form a ring structure. **a**, BamA POTRA 5 interacts with the C-terminal domain of BamD. BamA residues R366 and E373 and BamD residue R197 are important for the two protein interactions, and their carbon atoms are colored in yellow. **b**. BamA and BamB interaction. Both POTRA 2 and 3 involve in BamB interaction. BamA residues V245, Y255 and BamB residues L192, L194 and R195 play important roles in BamA and BamB interactions.

Figure 4 | BamE and BamC interact with BamA and BamD. a, The interface between BamE and BamA in the BamABCDE complex. BamE forms contacts with POTRA 5 residues, BamA periplasmic turns T-2 and T-3, and POTRA 4 in the BamACDE complex (Extended Data Fig. 6). **b**, The C-terminal globular domain of BamC interacts with BamA POTRA 2 at the β-sheets in BamACDE. Residues in the two β-sheets that are involved in the BamC and BamA interactions are shown.

Figure 5 | The function of BamA POTRA 5. **a**, The three β-strands of BamA POTRA 5. The residues selected for functional assays are shown: residues K351 and R353 on β1, T397, D399 and D401 on β2 and V415, K417 and K419 on β3. **b**, The β-strands of POTRA 5 are critical for the bacterial survive. The single mutant K351P, the double mutant K351P/R353P at β1, the double mutants V415P/K417P, K417P/K419P and V415P/K419P at β3 kill the bacteria, while the triple mutant T397P/D399P/D401P at β2 impairs cell growth. The protein expression of the BamA

wild-type and mutants. 1, 2, 3, 4, 5, 6, 7, 8, 9, 10, 11 and 12 represent the wild type BamA, the vector without BamA, BamA mutants K351P, R353P, K351P/R353P, T397P/D399P/D401P, V415P, K417P, K419P, V415P/K417P, K417P/K419P and V415P/K419P, respectively.

Figure legends for Extended Data Figures:

Extended Data Figure 1 | BamABCDE and BamACDE complexes and electron density maps contoured at 1 σ. a, Schematic diagram of the five BAM subunits. P-1 to P-5 represent the five BamA POTRA domains.**b**, SDS-PAGE analysis of the BAM complex from crystals. M, 1 and 2 are protein molecular weight marker, crystals of purified the BAM complex expressed by construct pYG120 and pJH114, respectively (Supplementary Data Figure 1). The BamABCDE crystals contain the full length BamA-E. The crystals were washed five times in fresh reservoir solution, and then dissolved in SDS-PAGE loading buffer. The results showed that the BamB is absent in the BamACDE crystals, while the BamC is complete in both the BamABCDE and BamACDE crystals. **c**, SDS-PAGE analysis of the purified BAM complex. M, 1 and 2 are protein molecular weight marker, purified BAM protein complex expressed by construct pYG120 and pJH114, respectively. The BAM complexes expressed from pJH114 is a mixture of BamABCDE and BamACDE complexes (Supplementary Data Figure 1). **d**, 2FoFc electron density map of BamA residues W576-K580 of BamACDE contoured at 1 σ. **e**, 2FoFC electron density map of BamD residues Y177-W191 of BamACDE contoured at 1 σ. **f**, 2FoFc electron density map of BamA residues Y504-Y509 and F490-F494 of BamABCDE complex contoured at 1σ. **g**, 2FoFc electron density map of BamB residues Y345-W348 contoured at 1 σ.

Extended Data Figure 2 | Superimposition of the two BamACDE complexes in the asymmetric unit. The BamACDE complex with the full length BamC, showing BamA (red), BamC (blue), BamD (magenta), and BamE (cyan). Only N-terminal loop of BamC was observed in another BamACDE complex in the asymmetric unit cell (yellow). The structure data suggests that the role of BamC is to retain the ring structure of BamA and BamD during OMP insertion. **a**, Membrane view of the superimposed BamACDE complexes. The primary difference is one complex has a complete BamC subunit, which binds BamD, BamE, POTRA 1 and 2, while the second complex only the N-terminal coil structure up to P88 is observed and the rest of BamC is disordered. The overall structures of the two complexes are very similar

with some conformational changes in the β-strands of barrel and extracellular loops with root-mean-square deviation (RMSD) of 0.908 Å over 378 Cα atoms, while the periplasmic circular structure has some rotation (see arrows) with a RMSD of 4.706 Å over 385 Cα atoms. **b**, Periplasmic view of the superimposition of the two structures. The periplasmic circular structure has some rotations when the C-terminal global domain binds on the POTRA 2. **c**. Superimposition of the barrels of the two complexes. **d**, Superimposition of the two BamCs. The N-terminal coil structures superimpose well with a RMSD of 0.807 Å over 86 Cα atoms.

Extended Data Figure 3 | Molecular dynamics simulation of BAM complexes. a, BamABCDE and **b,** BamACDE structures modelled with all subunits present and embedded in a model *E. coli* outer membrane (grey). Phosphate atoms are shown in orange spheres. Lipid-modified cysteine residues of BamB, BamC, BamD and BamE are shown in yellow spheres. **c**, Both complexes are stable in MD simulations, showing limited deviation from the starting configuration (shown in the background). **d**, Simulations of the complexes of only BamA and BamD subunits retain the ring structure. Without BamC present POTRA 1 (black circle) moves towards the membrane, while POTRA 3 (black arrow) moves towards and interacts with the periplasmic loops of the barrel. The dynamics of POTRA 3 appear to be modulated by BamB. **e**, Simulations of BamA show enhanced dynamics of the POTRA domains, with POTRA 1 and 2 rotating towards the membrane in an anti-clockwise direction (blue arrow). This separates POTRA 3 from the barrel (black arrow). This conformation of the POTRA domains is unable to form the BAM ring, highlighting the essential nature of BamD and its interactions with BamA in maintaining the ring structure.

Extended Data Figure 4 | BamA of the BamABCDE complex is superimposed onto the other published BamA structures. All the published BamA structures are in the inward-open conformation. In all cases the BamA from BamABCDE is shown in red. **a**, The BamA of BamABCDE complex is superimposed onto BamA of *N. gonorrhoeae* (grey) (protein data bank access code 4K3B)[18]. The two barrel structures are similar with a RMSD of 3.803 Å over 385 Cα atoms, but the conformations of the five POTRA domains are quite different. The dotted circle indicates the hydrophobic gap between β1C and β15C. **b**, BamA of *E. coli* (magenta) (PDB access code 4N75)[19]. The two barrel structures superimpose well with a RMSD of 0.644 Å over 385 Cα atoms, but differences are observed for the β16C terminal residues. The C-terminal residues in BamA of BamABCDE move toward to the lumen of the barrel. **c**, BamA of *E. coli* (yellow) (PDB access code 4C4V)[20] with a RMSD of 1.382 Å over 365 barrel Cα atoms. The conformations of the POTRA 5 are quite different. **d**, BamA of *H. ducreyi* (green) (PDB access code 4K3C)[18]. The barrel structures are similar with a RMSD of 2.376 Å over 365 barrel Cα atoms, but the conformations of POTRA 4 and 5 are quite different.

Extended Data Figure 5 | The conformational changes between the BamABCDE and BamACDE complexes and Heat-modifiability assays of the BamA double cysteine mutants. The two structures are superimposed onto the BamA barrel structures of BamABCDE and BamACDE complexes with a RMSD of 4.85 Å over

the 379 barrel Cα atoms and a maximum RMSD of 20 Å . The POTRA domains align with an RMSD of 5.764 Å over 384 Cα atoms with maximum 15 Å. The BamABCDE complex is in the same colour scheme as Figure 1. The BamACDE complex is in yellow. The barrel strands β1-6C rotate around 65° from BamABCDE to BamACDE, while the BAM periplasmic unit rotates around 30° in a counter-clockwise direction from BamABCDE to BamACDE. **a**, Membrane view of the superimposition of the BamABCDE and BamACDE complexes. The conformations of BamA POTRA domains, BamB, BamC and BamD are significantly different between the two complexes. **b**, The periplasmic view of the superimposition of BamABCDE and BamACDE. The circular units rotate around 30° between the two BAM complexes. **c**, The residues involved in closing the barrel at the periplasmic side in the BamACDE structure. d, Heat-modifiability assays of the BamA double cysteine mutants. SDS-PAGE/western blot analysis of the wild type BamA, BamA G393C/G584C, E435C/S665C and E435C/S658C mutants showed the heat-modifiability, indicating that the three double cysteine BamA mutants were correctly folded into the OM. U, F indicate unfolded and folded, respectively (Supplementary Data Figure S5).

Extended Data Figure 6 | Periplasmic loops bind to BamA POTRA 3, 5, BamD and BamE. In the BamABCDE complex, the BamA barrel interacts with POTRA 3, 5, BamE and BamD through the periplasmic turns T-1, -2, -3, -5, -6 and -7. **a**, In the BamABCDE complex, the residues of T-1, -2 and -3 are involved in the interactions with POTRA 5, BamD and BamE. **b**, Residues in T-5, -6 and -7 interact with POTRA 3 in the BamABCDE complex. **c**, In the BamACDE complex no interactions are observed between the periplasmic turns and POTRA 3. The figure shows that the residues in T-1, -2 and -3 interact with residues in POTRA 5, BamD and BamE. These structural data may suggest that BamB, C, D and E either directly or indirectly control the conformation of the barrel through its periplasmic turns.

Extended Data Figure 7 | BamA and BamD interactions, and Superimposition of the BamB structures and the conformational changes of POTRA2 and 3. **a**, BamA POTRA 1 and 2 interact with the N-terminal domain of BamD. The interacting residues from both BamA and BamD are shown. **b**, Functional assays of the BamA interaction with BamD. The mutation BamA E373K is lethal, while mutant R366E impairs the bacterial growth, suggesting these residues may play an important role in the BAM complex. 1, 2, 3, and 4 represent the wild type BamA, the vector without BamA, BamA mutants E373K and R366E, respectively. **c**, Protein expression levels of BamA mutations were detected by western blotting. **d**, Periplasmic view of BamB of the BamABCDE complex (green) superimposed onto the free BamB structure (orange) (PDB code 3Q7N)[21] with a RMSD of 1.81 Å over 351 Cα atoms with the maximum deviation of 12 Å at loop 19. Loops 15, 19, 23 and 27 of BamB adopt conformational changes to bind to POTRA 2 and 3. **e**, BamB of the BamABCDE complex superimposed onto BamB in complex with POTRA 3 and 4 (magenta) (PDB code 4PK1)[32]. The two BamB structures are very similar with a RMSD of 0.5860 Å over 341 Cα atoms. **f**, Superimposition of BamABCDE and BamACDE at POTRA 2 and 3 with a RMSD of 3.57 Å over 159 Cα atoms. In the BamACDE structure the hinge angle between POTRA 2 and 3 is reduced, while POTRA 2 and 3 also separate from BamB, reducing the the interactions between BamB, and POTRA 2 and 3.

Extended Data Figure 8 | BamE interacts with BamD and BamC, and BamC interactions with BamD. BamE interacts with BamA, BamD and BamC. BamC binds extensively to the C-terminal domain of BamD. **a**. BamE interacts with BamD in the BamACDE complex. BamE contacts the C-terminal domain residues of BamD in the BamACDE complex. **b**, BamE forms hydrophobic interactions with BamC in the BamACDE complex. BamE residues P67, F68 and BamC residues M56 and I57 are shown. **c**, BamC forms contacts with BamA POTRA 1 in BamACDE. BamA residues F31, Q35, V39 and BamC residues G94 and R96 are shown. **d**, BamC interacts with the C-terminal domain of BamD. The interacting residues are shown as sticks. **e**, BamC interacts with the N-terminal domain of BamD.

Extended Data Figure 9 | Conserved residues analysis of BAM complex. Consurf residue conservation scores (1-9), plotted onto the molecular surfaces as a colour scale for BamA (red), BamB (green), BamC (blue), BamD (purple) and BamE (cyan), for the BamABCDE structure. Regions of white/grey indicate poorly conserved residues, whereas a more intense colour indicates highly conserved residues. Black dashed circles represent the interaction points on removal of BamC (a), BamD (b), BamE (c) and BamB (d). For each interaction patch a high density of conserved residues is apparent.

Extended Data Figure 10 | Conformational differences of the BAM subunits between the BamABCDE and BamACDE complexes, and BAM complex interacts with lipid of the OM. The subunits of BamABCDE are colored in the same colours as Figure 1, while the BamACDE subunits are in yellow. **a**, Superimposition of the BamA subunits onto the barrel domain with an RMSD of 4.85 Å over the 379 barrel Cα atoms and an RMSD of 5.76 Å over the 384 Cα atoms of the POTRA domains. The BamA barrel has significant conformational changes in β1C-β6C. The periplasmic POTRA domains rotate about 30° from BamABCDE complex to BamACDE complex, suggesting a novel rotation mechanism to facilitate OMP insertion into the OM. **b**, Superimposition of the BamC structures. The BamC structures have some conformational changes with a RMSD of 2.102 Å over 47 Cα atoms of the BamC N-terminal loop. The N-terminal loop C25-V35 becomes more ordered in BamACDE complex. Particularly, the N-terminal domain and the C-terminal domain are ordered and bind to POTRA 1, 2 and the N-terminal domain of BamD in BamACDE complex. The N-terminal loops of the BamC structures superimpose well between residues V35 to P88. **c**, Superimposition of the BamD structures with an RMSD of 1.201 Å over 203 Cα atoms. The α-helices are conserved, but the loops have some conformational changes, especially loop 6 (residues D121-D136) between α-helix 5 and α-helix 6. **d**, Superimposition of BamE structures with a RMSD of 1.721 Å over 81 Cα atoms. The β strands and α-helices of BamE are well conserved, with minor conformational changes observed in the loops. **e,** Lipid-protein interactions for the BamACDE structure. BamB was modelled into the BamACDE complex by molecular modelling. The BamABCDE complex was built in the OM (Methods), and the residues interacting with lipids of the OM with 4 Å are shown in putty representation to depict lipid interaction residues. Equivalent residues in all five subunits BamA (red), BamB (green), BamC (blue), BamD (purple) and BamE (cyan) interact with the membrane in all three independent simulations. **f,** Lipid-protein interactions for the BamABCDE structure. BamC was added to the

BamABCDE complex by molecular modelling, using the solved domain from the companion complex. BamABCDE complexe was inserted into the OMP, with lipid anchors designed (Methods).

Extended Data Table 1 | Data collection and refinement statistics.

Online Content Full methods, along with any additional Extended Data display items and Source Data, are available in the online version of the paper; references unique to these sections appear only in the online paper.

METHODS

Cloning, expression and purification of BAM complex

Expression plasmid pJH114 containing the five *E. coli bamABCDE* genes which were under the control of a trc promoter, and with an octa-histidine (8×His) tag at the C-terminus of *bamE* was initially used for overexpression of BamABCDE complex in *E. coli* HDB150 cells[16]. Expression of the native BamABCDE complex was induced with 100 μmol l^{-1} Isopropyl-β-D-1-thiogalactopyranoside (IPTG; Formedium) at 20°C overnight when the optical density of the cell culture at 600 nm reached 0.5-0.8. The selenomethionine-labeled BAM complexes were expressed in M9 medium supplemented with selenomethionine Medium Nutrient Mix (Molecular Dimensions) and 100 mg l^{-1} L-(+)-selenomethionine (Generon Ltd) using the similar conditions as the native BamABCDE.

Both native and selenomethionine-labelled BamABCDE complexes were purified using a similar protocol. Briefly, the cells were pelleted and resuspended in lysis buffer containing 20 mM Tris-HCl, pH 8.0, 150 mM NaCl, 10 μg ml^{-1} DNase I and 100 μg ml^{-1} lysozyme and lysed by passing through a cell disruptor (Constant

Systems Ltd) at 30 kpsi. The lysate was centrifuged to remove the cell debris and unbroken cells, and the supernatant was ultracentrifuged to pellet the membranes at 100,000g for 1 h. The cell membranes were resuspended in solubilization buffer containing 20 mM Tris-HCl, pH 8.0, 300 mM NaCl, 10 mM imidazole and 1~2% n-Dodecyl-β-D-Maltopyranoside (DDM; all detergents were purchased from Anatrace) and rocked for 1 h at room temperature or overnight at 4°C. The suspension was ultracentrifuged and the supernatant was applied to a 5 mL pre-equilibrated HisTrap HP column (GE Healthcare). The column was washed with wash buffer containing 20 mM Tris-HCl, pH 8.0, 300 mM NaCl and 35 mM imidazole and eluted with elution buffer containing 300 mM imidazole. The eluent was applied to HiLoad 16/600 Superdex 200 prep grade column (GE healthcare) pre-equilibrated with gel filtration buffer containing 20 mM Tris-HCl, pH 7.8, 300 mM NaCl and detergents. Different detergents were used in protein purification procedures.

The purified BamABCDE complex was analyzed by SDS-PAGE (Extended Data Figure 1 and Supplementary Data Figure 1), which indicated that BamB is not enough in the complex, and BamB is absent in the determined structure. We therefore decided to generate a new plasmid to express the BamABCDE complex. Additional copy of *E. coli bamB* gene was introduced into pJH114[16] after the 8×His tag to generate a new expression plasmid pYG120 using a modified sequence and ligation-independent cloning (SLIC) method[42]. In brief, vector backbone and *bamB* gene fragments were amplified by polymerase chain reaction (PCR) using Q5® Hot Start High-Fidelity DNA Polymerase (New England BioLabs), and plasmid pJH114 as template and primers PF_pJH114_SLIC (5'-GTTAATCGACCTGCAGGCATGCAAG-3') and PR_pJH114_SLIC (5'-

CTCTAGAGGATCTTAGTGGTGATGATGGTG-3'), and PF_EBB_SLIC (5'-TCATCACCAC-TAAGATCCTCTAGAGAGGGACCCGATGCAATTGC-3') and PR_EBB_SLIC (5'-CTTGC-ATGCCTGCAGGTCGATTAACGTGTAATAGAGTACACGGTTCC-3'), respectively. Gel extracted fragments were digested by T4 DNA polymerase (Fermentas) at 22°C for 35 min followed by 70°C for 10 min, and then placed on ice immediately. The digested fragments were annealed in an annealing buffer (10 mM Tris, pH 8.0, 100 mM NaCl and 1 mM EDTA) by incubating at 75°C for 10 min and decreasing by 0.1°C every 8 seconds to 20°C. The mixture was transformed into *E. coli* DH5α for plasmid preparation. The DNA sequences were confirmed by sequencing.

For the purification of the BamABCDE complex from the pYG120 construct, the wash buffer, elution buffer and gel filtration buffer were supplemented with different detergent combinations. A second gel filtration was performed to change detergents with gel filtration buffer containing 1 CMC n-Octyl-β-D-Glucopyranoside (OG) and 1 CMC n-Dodecyl-N,N-Dimethylamine-N-Oxide (LDAO). For BamABCDE complex purification from construct pJH114, the wash buffer, elution buffer and gel filtration buffer were supplemented with 2 CMC n-Nonyl-β-d-glucoside (β-NG) and 1 CMC Tetraethylene Glycol Monooctyl Ether (C8E4). The peak fraction was pooled and concentrated using Vivaspin 20 centrifugal concentrator (Sartorius, molecular weight cut off: 100 kDa). The selenomethionine-labeled proteins were purified in the same way as the native proteins of BamABCDE complex.

Crystallization, data collection and structure determination

The purified proteins were concentrated to 8~12 mg ml^{-1} for crystallization. For NaI co-crystallization, NaCl was replaced by NaI in the gel filtration buffer. All

crystallizations were carried out by sitting-drop vapour diffusion method in the MRC 96 well crystallization plates (Molecular Dimensions) at 22 °C. The protein solution was mixed in a 1:1 ratio with the reservoir solution using the Gryphon crystallization robot (Art Robbins Instruments). The best NaI co-crystallized crystals were grown from 150 mM HEPES, pH 7.5, 30% PEG6000 and CYMAL®-4 in MemAdvantage™ (Molecular Dimensions) as additive. The best native crystals were grown from 150 mM HEPES, pH 7.5 and 27.5% PEG6000. The best selenomethionine-labeled crystals were grown from 100 mM Tris, pH 8.0, 200 mM $MgCl_2 \cdot 6H_2O$, 24% PEG1000 MME and OGNG in MemAdvantage™ as additive. The crystals were harvested, flash-cooled and stored in liquid nitrogen for data collection. The data sets of selenomethionine labelled BAM complex were collected on the I03 beamline at Diamond Light Resources (DLS) at a wavelength of 0.9795 Ångström (Å). All data were indexed, integrated and scaled using XDS[43]. The crystals belong to space group of $P4_22_12$, with the cell dimensions a = b = 254.16 Å, c = 179.22, $\alpha = \beta = \gamma = 90°$. There are two complexes in the asymmetric unit. The structure was determined to 3.9 Å resolution (Extended Data Table 1) using ShelxD[44,45]. Fifty-six selenium sites were found, which gave a FOM of 0.32. Following density modification using DM[46], the BamACDE complex was clearly visible in the electron density map, but without BamB. Using the individual high-resolution models, the BamACDE complex was built using Coot[47] by skeletonizing the electron density map and docking the BAM subunits in the electron density map with selenomethionine sites used as guides. Rigid body refinement was performed following manual docking. NCS refinement was used along with TLS refinement against groups automatically determined using PHENIX[48]. Restrained refinement was performed with group B-factors alongside

reference model secondary structure restraints from higher resolution models. Weights were automatically optimised by PHENIX[48].

To obtain the BamABCDE complex structure, the new construct was used to produce sufficient BamB to form the BamABCDE complex. The data sets of BamABCDE complex were collected on the I02 beamline at DLS. The crystals belong to space group $P4_12_12$, with the cell dimensions a = b = 116.69 Å, c = 435.19 Å, $\alpha=\beta=\gamma=90°$. There is one complex molecule in the asymmetric unit. Although the crystals diffracted to 2.90 Å, the crystal structure of BamABCDE could not be determined by molecular replacement. BamABCDE complex was crystallized in presence of 0.2 M sodium iodide, and SAD datasets were collected at a wavelength of 1.8233 Å. 4 x 360 degree datasets were collected on different regions of the same crystal of NaI co-crystallization then combined. The phases were determined by ShelxD[44,45] at 4 Å resolution. Eleven iodide sites were found, which gave a FOM of 0.28. The phases were extended to 2.90 Å by DM[46], and the model was built using Coot[47] by skeletonizing the electron density map and docking the individual high-resolution subunits in the electron density map and rigid body fit this model into the higher resolution native dataset while retaining and extending the free R set from the iodide dataset. The BamABCDE complex was refined using PHENIX[48]. TLS groups were automatically determined using PHENIX[48] and used for refinement along with individual B-factors. Weights were automatically optimised and secondary structure restraints were used.

Site-directed mutagenesis and functional assays

An E. coli bamA expression plasmid was constructed for functional assays using SLIC method as described above. An N-terminal 10×His tag fused with bamA starting from residue 22 was amplified by PCR using Q5® Hot Start High-Fidelity

DNA Polymerase (New England BioLabs), and plasmid pJH114 as template and primers PF_bamA_SLIC (CCATCATCATCATCATCATC-ATCATGAAGGGTTCGTAGTGAAAGATATTCATTTCGAAG) and PR_bamA_SLIC (AGA-CTCGAGTTACCAGGTTTTACCGATGTTAAACTGGAAC). Vector backbone was amplified from a modified pRSFDuet™-1 vector (Novagen, Merck Millipore) containing an N-terminal pelB signal peptide coding sequence with primers PF_RSFM_SLIC (CGGTAAAACCTGGTAACTC-GAGTCTGGTAAAGAAACCGCTGC) and PR_RSFM_SLIC (ATGATGATGATGATGATG-ATGATGGTGATGGGCCATCGCCGGCTG). Plasmids were prepared using GeneJET Plasmid Miniprep Kit (Thermo Scientific). Site-directed mutagenesis was performed according to a previously described protocol[49] with slight modification (PCR conditions and the sequences of the primers are available upon request). The sequences of the wild type and all mutant constructs of bamA were confirmed by sequencing. *E. coli* JCM166 cells[3] transformed with the wild-type bamA or its mutants were plated on LB agar plates supplemented with 50 μg ml^{-1} kanamycin and 100 μg ml^{-1} carbenicillin in the presence or absence of 0.05% L-(+)-arabinose and grown overnight at 37°C. Single colonies grown on arabinose-containing plates were inoculated in 10 ml LB medium supplemented with 50 μg ml^{-1} kanamycin, 100 μg ml^{-1} carbenicillin and 0.025% L-(+)-arabinose, and incubated at 200 rpm at 37°C for 16 h. For plate assays, the cells were pelleted and resuspended in fresh LB medium supplemented with 50 μg ml^{-1} kanamycin and 100 μg ml^{-1} carbenicillin, and diluted to an absorbance (A_{600} nm) of ~0.3 and streaked onto LB agar plates supplemented with 50 μg ml^{-1} kanamycin, 100 μg ml^{-1} carbenicillin in the presence or absence of 0.05% L-(+)-arabinose and cultured at 37°C for 12-14 h.

Western blot

Western blotting was performed to examine protein expression levels of BamA in the membrane. 50 ml of overnight cultures of transformed JCM166 cells with respective wild-type or each mutant of BamA were pelleted. The cells were resuspended in 25 ml 20 mM Tris-HCl (pH 8.0), 150 mM NaCl and sonicated. The cell debris and unbroken cells were removed by centrifugation at 7,000 g for 30 min. The supernatant was centrifuged at 100,000 g for 60 min and the membrane fraction was collected. The membrane fraction was suspended in 5 ml buffer containing 20 mM Tris-HCl (pH 8.0), 150 mM NaCl and 1% 3-(N,N-Dimethylmyristylammonio) propanesulfonate (Sigma) and solubilized for 30 min at room temperature. Samples were mixed with 5 × SDS-PAGE loading buffer, heated for 5 min at 90 °C, cooled for 2 min on ice and centrifuged. Ten microliters of each sample was loaded onto 4-20% Mini-PROTEAN® TGX™ Gel (Bio-Rad) for SDS-PAGE and then subjected to immunoblot analysis.

The proteins were transferred to PVDF membrane using Trans-Blot® Turbo™ Transfer Starter System (Bio-Rad) according to the manufacturer's instructions. The PVDF membranes were blocked in 10 mL Protein-free T20 (TBS) blocking buffer (Fisher) overnight at 4°C. The membranes were incubated with 10 mL His•Tag® Monoclonal Antibody (diluted, 1:1000) (Millipore) for 1 h at room temperature followed by washed with PBST for 4 times and incubated with IRDye 800CW goat anti-mouse IgG (diluted, 1:5000) (LI-COR) for 1 h. The membrane was washed with PBST for 4 times and PBS for 2 times. Images were acquired using LI-COR Odyssey (LI-COR).

BamA Heat-modifiability assays

The JCM166 cells containing the double cysteine mutants G393C/G584C, E435C/S665C and E435C/S658C of BamA were cultured overnight in LB medium with 50 μg ml^{-1} kanamycin, 100 μg ml^{-1} carbenicillin and 0.025% L-(+)-arabinose, respectively. The membrane fraction from 50 ml cells was isolated and solubilized as described above. The samples were mixed with SDS loading buffer and then boiled for 5 min or kept at room temperature for 5-10 min. SDS-PAGE was performed at 4°C by running the gel for 60 min at 150 V. The proteins were transferred to PVDF membrane as described above and the BamA mutants were detected by western blotting.

Molecular modelling and simulations

All Molecular dynamics simulations (MDS) were performed using GROMACS v5.0.2[50]. The Martini 2.2 force field[51] was used to run an initial 1 μs Coarse Grained (CG) MD simulation to permit the assembly and equilibration of a 1-palmitoly, 2-cis-vaccenyl, phosphatidylglycerol (PVPG): 1-palmitoly, 2-cis-vaccenyl, phosphatidylethanolamine (PVPE) bilayers around the BamABCDE complexes[52]. Using the self-assembled system as a guide the coordinates of the BAM complexes were inserted into an asymmetric model *E. coli* OM, comprised of PVPE, PVPG, Cardiolipin in the periplasmic leaflet and the inner core of Rd1 LPS lipids in the outer leaflet[53], using Alchembed[54]. This equated to a total system size of ~500,000 atoms. The systems were then equilibrated for 1 ns with the protein restrained before 100 ns of unrestrained atomistic MD using the Gromos53a6 force field[55]. The lipid-modified cysteine parameters were created from lipid parameters for diacylglycerol and palmitoyl and appended to the parameters of the N-terminal cysteines[56]. Systems were neutralised with Mg^{2+}

ions, to preserve the integrity of the outer leaflet of the OM, and a 150 mM concentration of NaCl.

All ~500,000 atom systems were all run for 100 ns, with box dimensions in the region of 200x200x150 $Å^3$. To assess the stability of the subunit stoichiometry we assessed various combinations of BAM assemblies. For both BamACDE and BamABCDE crystal structures, we investigated ABCDE, AD and A alone, with 3 repeats each; while single simulations were also performed for BamABD, ACD, ADE, ABDE and ACDE, with a total simulation time equating to 2.8 μs. In cases where domains or subunits were missing these were added to the complex by structurally aligning the resolved units from the companion structure. For BamB, this was added to the BamACDE complex by structurally aligning POTRA 3. For the full BamC, this was added to the BamABCDE by aligning the resolved N-termainal domains. Individual protein complexes were configured and built using Modeller[57] and Pymol[58]. All simulations were performed at 37°C, with protein, lipids and solvent separately coupled to an external bath, using the velocity-rescale thermostat[59]. Pressure was maintained at 1 bar, with a semi-isotropic compressibility of 4 x 10^{-5} using the Parinello-Rahman barostat[60]. All bonds were constrained with the LINCS algorithm[61,62]. Electrostatics was measured using the Particle Mesh Ewald (PME) method[63], while a cut-off was used for Lennard-Jones parameters, with a Verlet cut-off scheme to permit GPU calculation of non-bonded contacts. Simulations were performed with an integration timestep of 2 fs.

The linear interpolation between the three structures was performed using the morph operation in Gromacs tools[50]. Analysis of the molecular simulations was performed using Gromacs tools[50], MDAnalysis[64] and locally written scripts.

Conservation analysis was performed using Consurf[65]. For each subunit, 150 homologues were collected from UNIREF90[66] using three iterations of CSI-Blast[67], with an E-value of 0.0001. The Consurf scores were then mapped into the B-factor column for each of the subunits.

REFERENCES

42 Li, M. Z. & Elledge, S. J. Harnessing homologous recombination in vitro to generate recombinant DNA via SLIC. *Nat. Methods* **4**, 251-256 (2007).

43 Kabsch, W. Xds. *Acta Crystallogr. D* **66**, 125-132 (2010).

44 Sheldrick, G. M. Experimental phasing with SHELXC/D/E: combining chain tracing with density modification. *Acta Crystallogr. D* **66**, 479-485 (2010).

45 Karplus, P. A. & Diederichs, K. Linking Crystallographic Model and Data Quality. Science 336, 1030-1033 (2012).

46 Cowtan, K. dm: An automated procedure for phase improvement by density modification. *Joint CCP4 and ESF-EACBM Newsletter on Protein Crystallography*. **31**, 34-38 (1994).

47 Emsley, P., Lohkamp, B., Scott, W. G. & Cowtan, K. Features and development of Coot. *Acta Crystallogr. D* **66**, 486-501 (2010).

48 Adams, P. D. *et al*. PHENIX: a comprehensive Python-based system for macromolecular structure solution. *Acta Crystallogr. D* **66**, 213-221(2010).

49 Liu, H. & Naismith, J. H. An efficient one-step site-directed deletion, insertion, single and multiple-site plasmid mutagenesis protocol. *BMC Biotechnol.* **8**, 91 (2008).

50 Pronk, S. *et al*. GROMACS 4.5: a high-throughput and highly parallel open source

molecular simulation toolkit. *Bioinformatics* **29**, 845-854 (2013).

51 de Jong, D. H. *et al*. Improved parameters for the Martini coarse-grained protein force field. *J. Chem. Theory Comput.* **9**, 687-697 (2013).

52 Stansfeld, P. J. *et al*. MemProtMD: Automated insertion of membrane protein structures into explicit lipid membranes. *Structure* **23**, 1350-1361 (2015).

53 Piggot, T. J., Pineiro, A. & Khalid, S. Molecular dynamics simulations of phosphatidylcholine membranes: a comparative force field study. *J. Chem. Theory Comput.* **8**, 4593-4609 (2012)

54 Jefferys, E., Sands, Z. A., Shi, J. Y., Sansom, M. S. P. & Fowler, P. W. Alchembed: a computational method for incorporating multiple proteins into complex lipid geometries. *J. Chem. Theory Comput*. **11**, 2743-2754 (2015).

55 Oostenbrink, C., Villa, A., Mark, A. E. & Van Gunsteren, W. F. A biomolecular force field based on the free enthalpy of hydration and solvation: The GROMOS force-field parameter sets 53A5 and 53A6. *J. Comput. Chem.* **25**, 1656-1676 (2004).

56 Domanski, J., Stansfeld, P. J., Sansom, M. S. P. & Beckstein, O. Lipidbook: A Public Repository for Force-Field Parameters Used in Membrane Simulations. *J. Membrane. Biol.* **236**, 255-258 (2010).

57 Eswar, N. *et al*. Comparative protein structure modeling using MODELLER. *Curr. Protoc. Bioinformatics* **15**, 5.6.1-5.6.30 (2006).

58 The PyMOL Molecular Graphics System, Version 1.8 Schrödinger, LLC.

59 Bussi, G., Zykova-Timan, T. & Parrinello, M. Isothermal-isobaric molecular dynamics using stochastic velocity rescaling. *J. Chem. Phys.* **130**, (2009).

60 Parrinello, M. & Rahman, A. Polymorphic Transitions in Single-Crystals - a New Molecular-Dynamics Method. *J. Appl. Phys.* **52**, 7182-7190 (1981).

61 Hess, B., Kutzner, C., van der Spoel, D. & Lindahl, E. GROMACS 4: Algorithms for highly efficient, load-balanced, and scalable molecular simulation. *J. Chem. Theory Comput.* **4**, 435-447 (2008).

62 Hess, B. GROMACS 4: Algorithms for highly efficient, load-balanced, and scalable molecular simulation. *Abstr. Pap. Am. Chem. S.* **237**, (2009).

63 York, D. M., Wlodawer, A., Pedersen, L. G. & Darden, T. A. Atomic-Level Accuracy in Simulations of Large Protein Crystals. *Proc. Natl Acad. Sci. USA* **91**, 8715-8718 (1994).

64 Michaud-Agrawal, N., Denning, E. J., Woolf, T. B. & Beckstein, O. Software News and Updates MDAnalysis: A Toolkit for the Analysis of Molecular Dynamics Simulations. *J. Comput. Chem.* **32**, 2319-2327 (2011).

65 Ashkenazy, H., Erez, E., Martz, E., Pupko, T. & Ben-Tal, N. ConSurf 2010: calculating evolutionary conservation in sequence and structure of proteins and nucleic acids. *Nucleic Acids Res.* **38**, W529-W533 (2010).

66 Suzek, B. E. *et al*. UniRef clusters: a comprehensive and scalable alternative for improving sequence similarity searches. *Bioinformatics* **31**, 926-932 (2015).

67 Biegert, A. & Soding, J. Sequence context-specific profiles for homology searching. *Proc. Natl Acad. Sci. USA* **106**, 3770-3775 (2009).

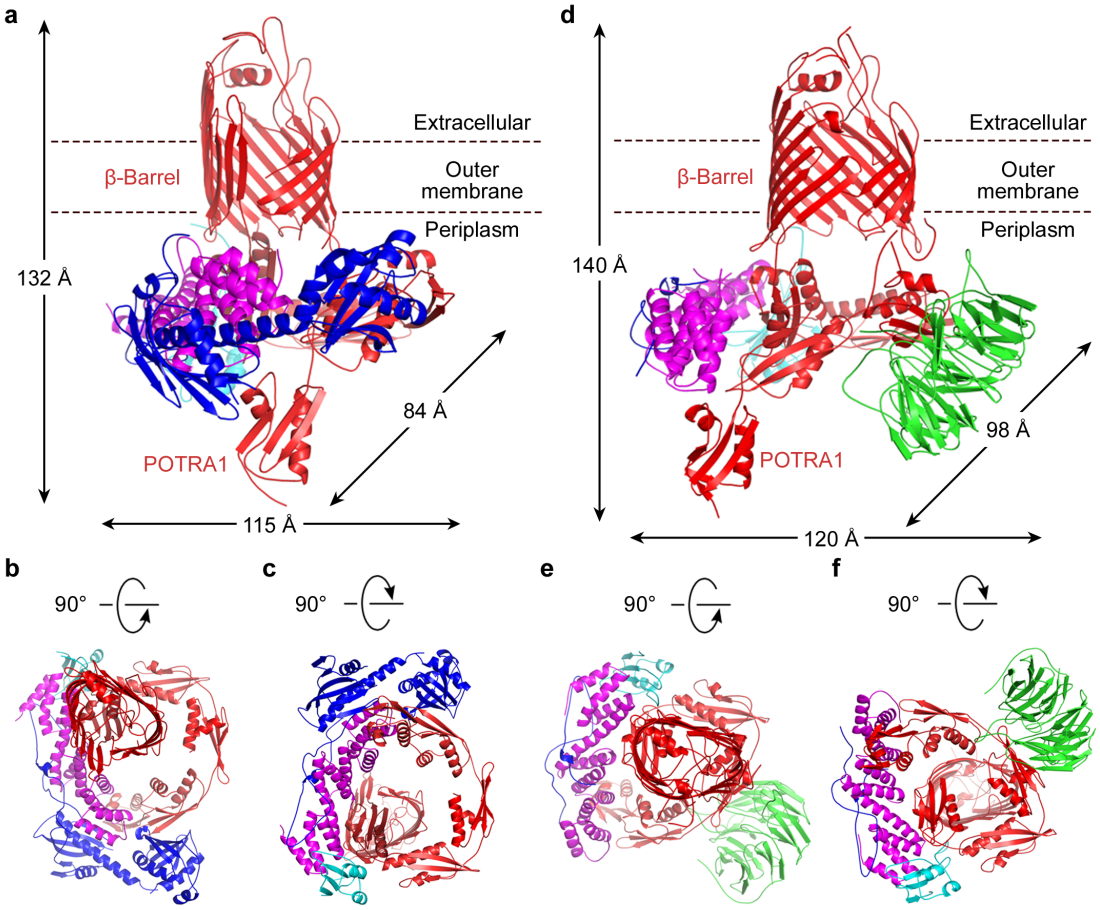
a
Extracellular
β-Barrel
Outer membrane
Periplasm
132 Å
84 Å
POTRA1
115 Å
d
Extracellular
β-Barrel
Outer membrane
Periplasm
140 Å
98 Å
POTRA1
120 Å
b
90°
c
90°
e
90°
f
90°

Figure 1

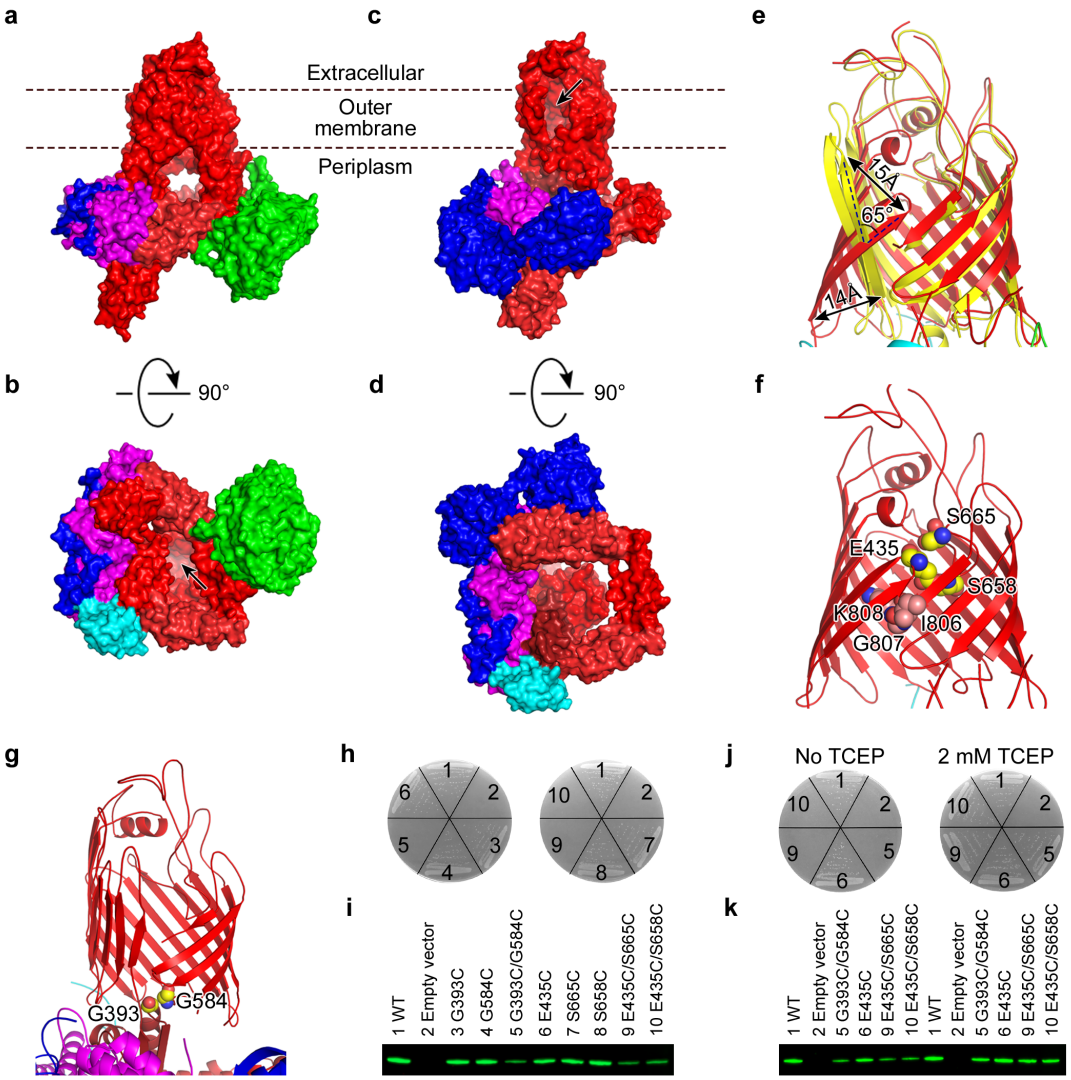
a
c
e
Extracellular
Outer
membrane
Periplasm
15Å
65°
14Å
b
90°
d
90°
f
S665
E435
S658
K808
I806
G807
g
G393
G584
h
1
2
3
4
5
6
7
8
9
10
i
1 WT
2 Empty vector
3 G393C
4 G584C
5 G393C/G584C
6 E435C
7 S665C
8 S658C
9 E435C/S665C
10 E435C/S658C
j
No TCEP
2 mM TCEP
k
1 WT
2 Empty vector
5 G393C/G584C
6 E435C
9 E435C/S665C
10 E435C/S658C

Figure 2

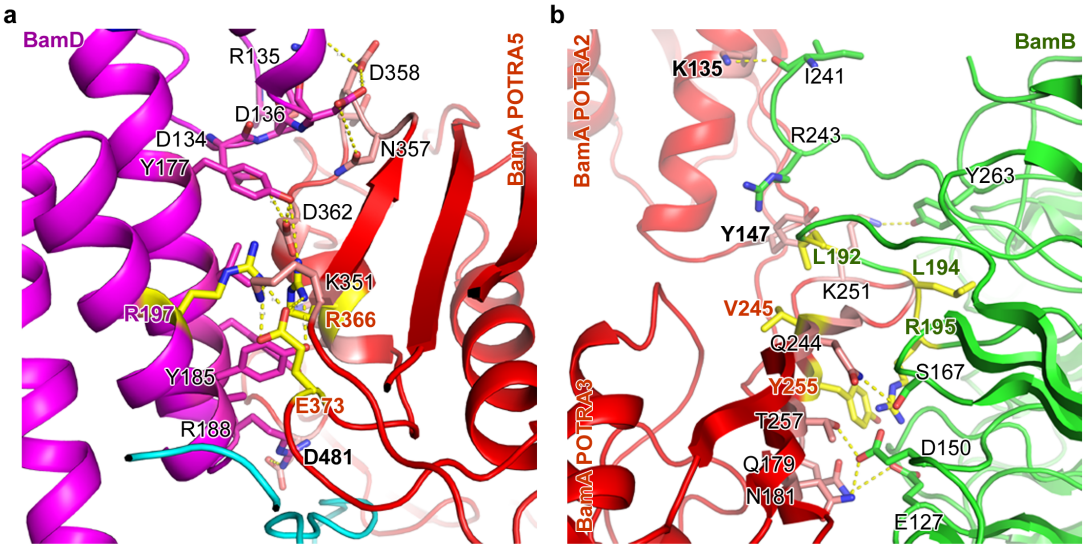
a
BamD
R135
D358
D136
D134
N357
Y177
BamA POTRA5
D362
K351
R197
R366
Y185
E373
R188
D481
b
BamA POTRA2
BamB
K135
I241
R243
Y263
Y147
L192
L194
K251
V245
R195
Q244
S167
Y255
T257
D150
Q179
N181
E127
BamA POTRA3

Figure 3

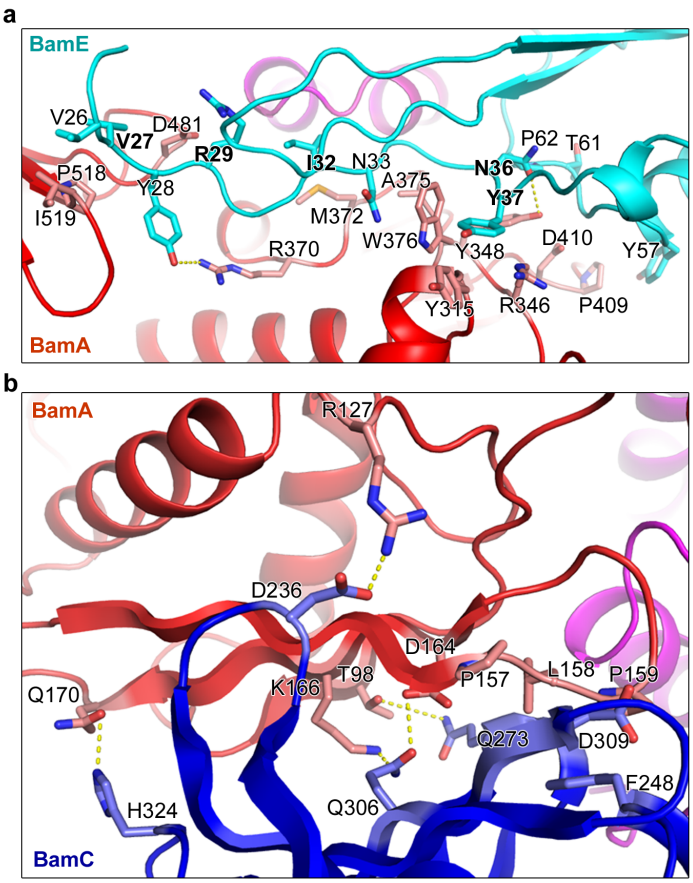
a
BamE
V26
D481
V27
R29
I32
N33
P62
T61
P518
Y28
A375
N36
Y37
I519
M372
R370
W376
Y348
D410
Y57
Y315
R346
P409
BamA
b
BamA
R127
D236
D164
T98
P157
L158
P159
Q170
K166
Q273
D309
F248
H324
Q306
BamC

Figure 4

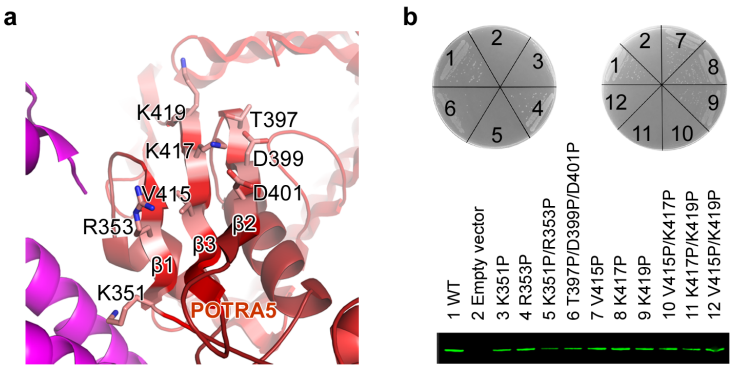
a
K419
T397
K417
D399
V415
D401
R353
β2
β3
β1
K351
POTRA5
b
1 WT
2 Empty vector
3 K351P
4 R353P
5 K351P/R353P
6 T397P/D399P/D401P
7 V415P
8 K417P
9 K419P
10 V415P/K417P
11 K417P/K419P
12 V415P/K419P

Figure 5

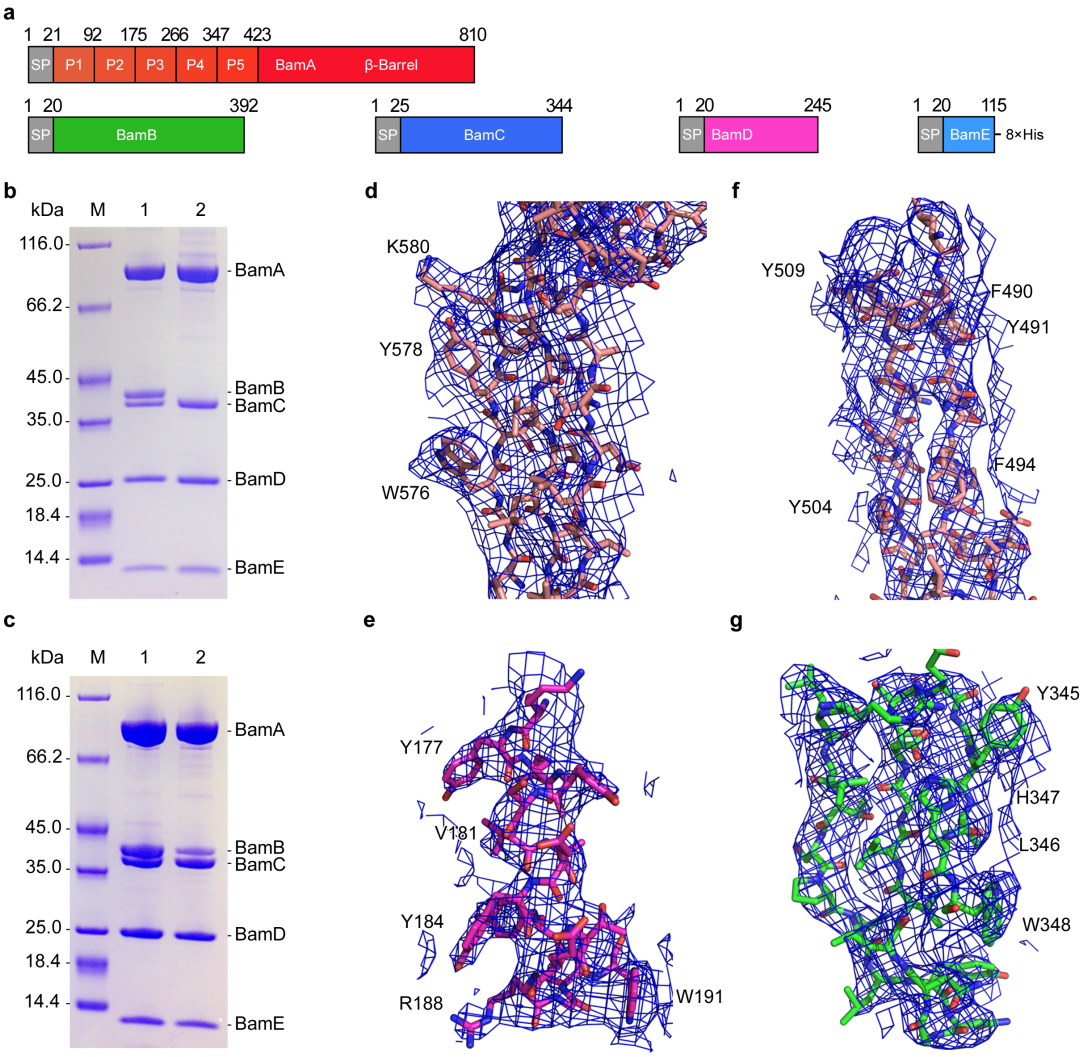

Extended Data Figure 1

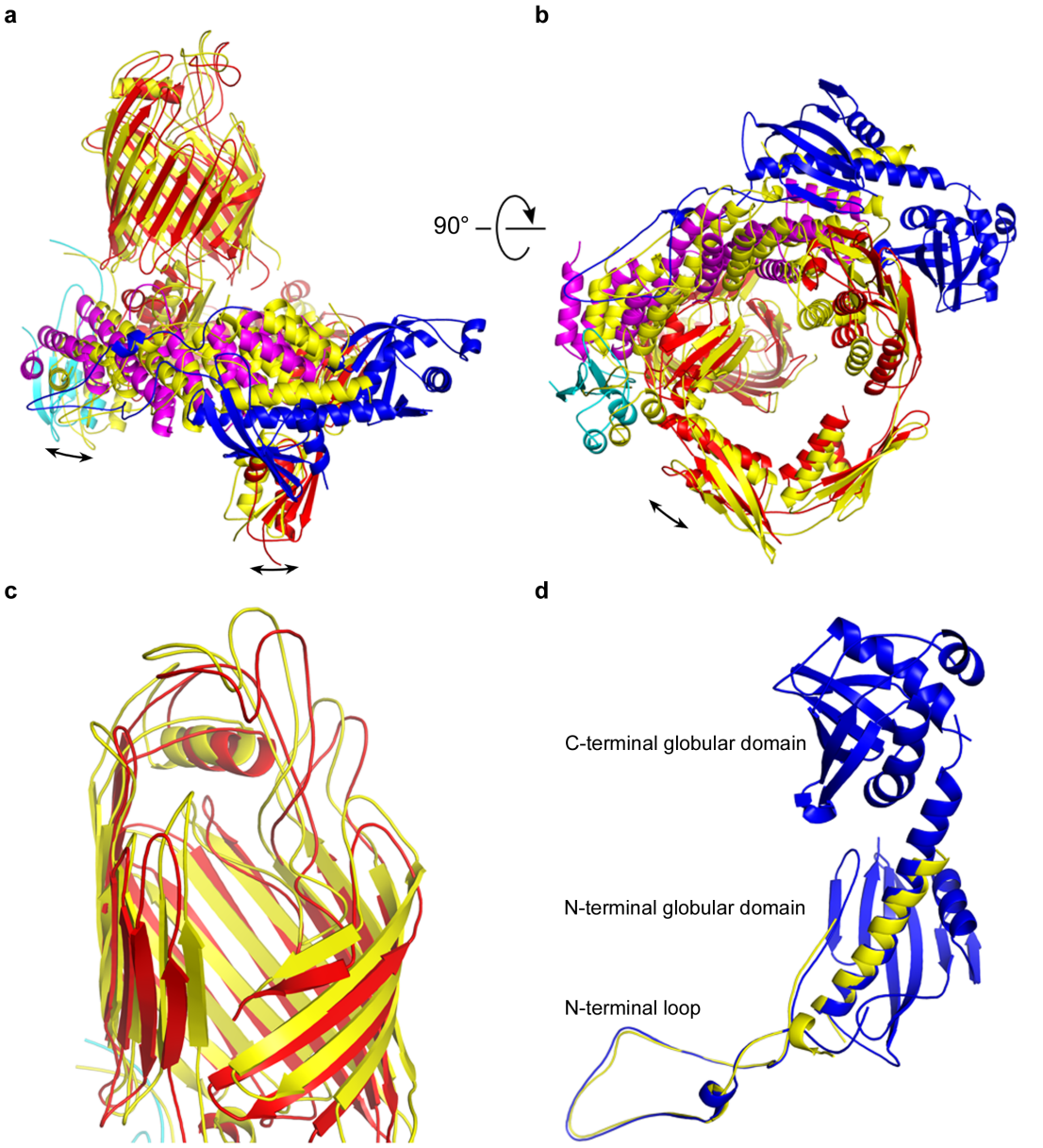

Extended Data Figure 2

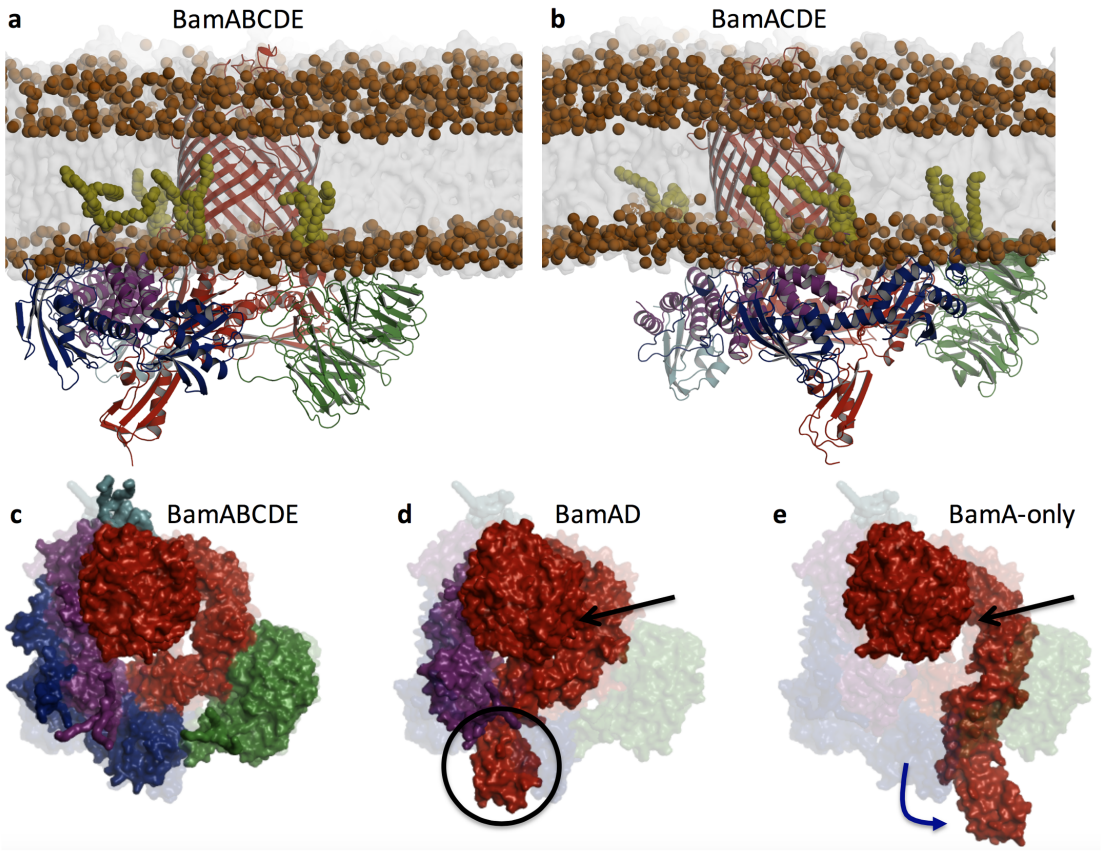

Extended Data Figure 3.

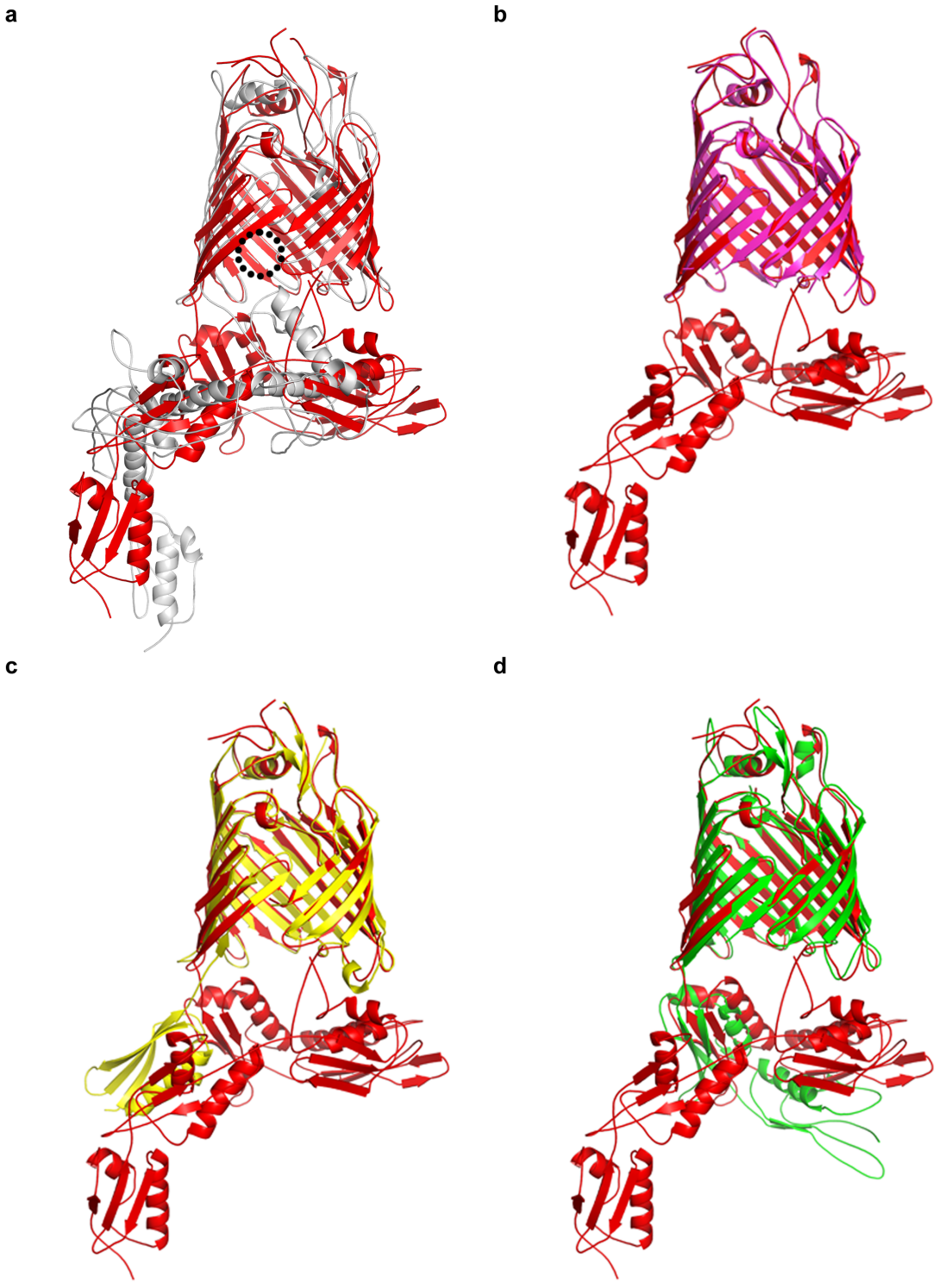

Extended Data Figure 4

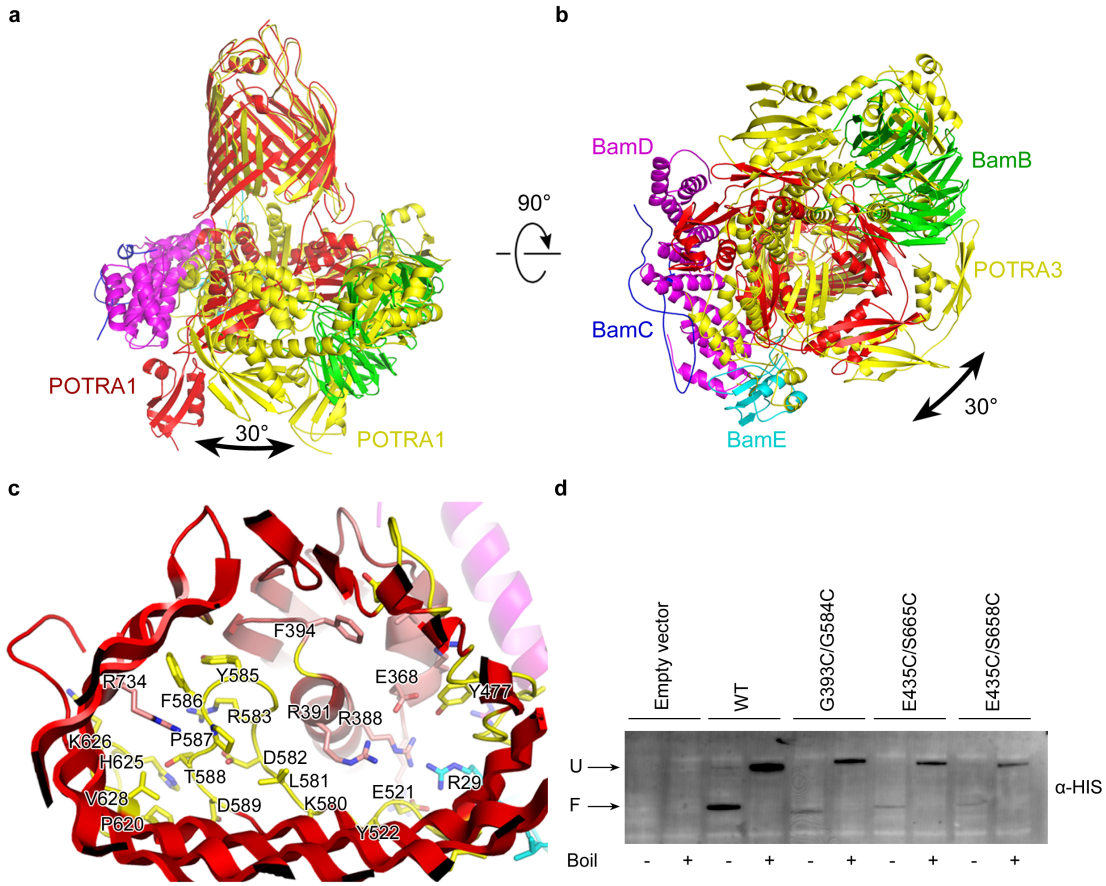

Extended Data Figure 5

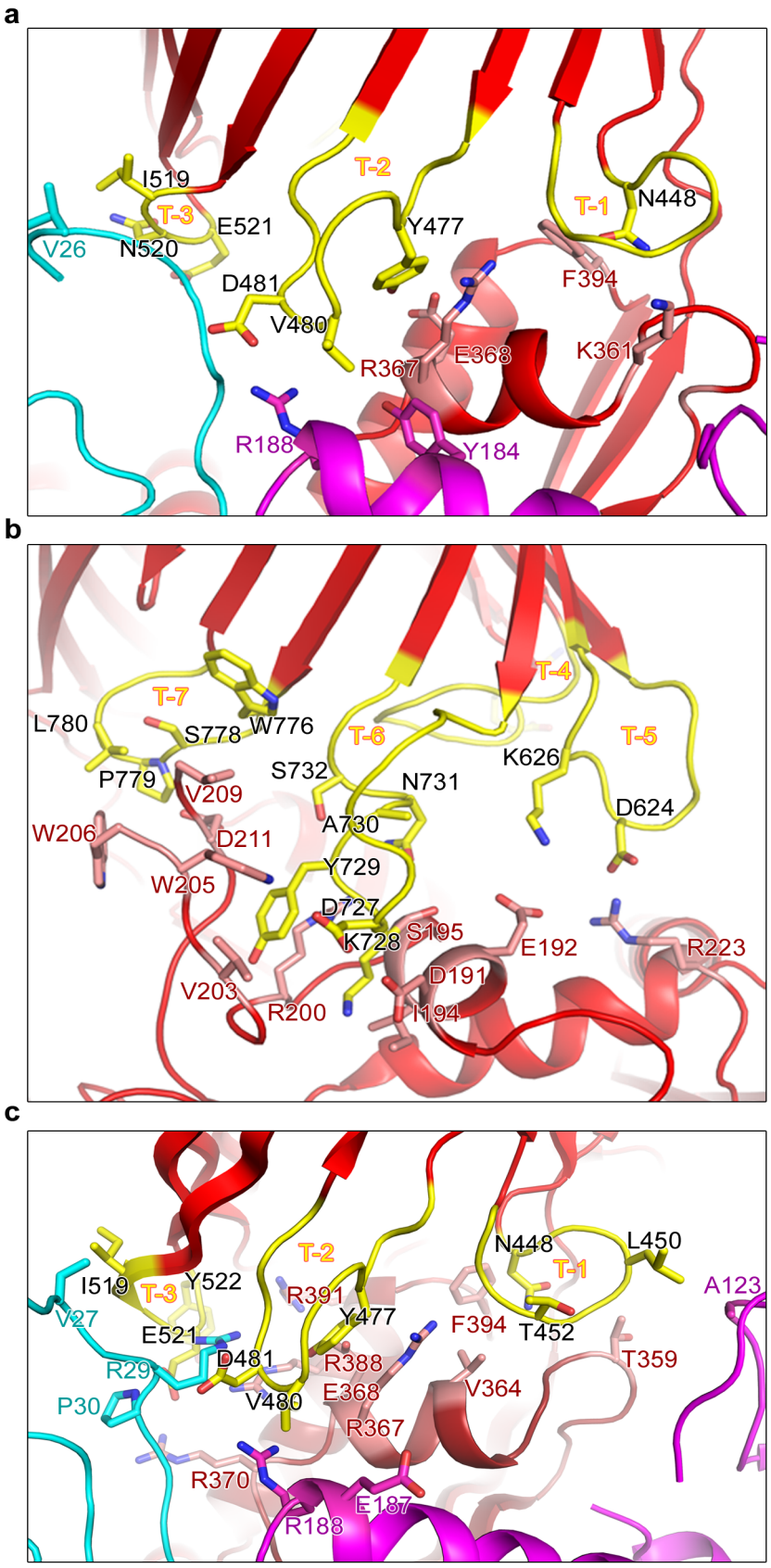

Extended Data Figure 6

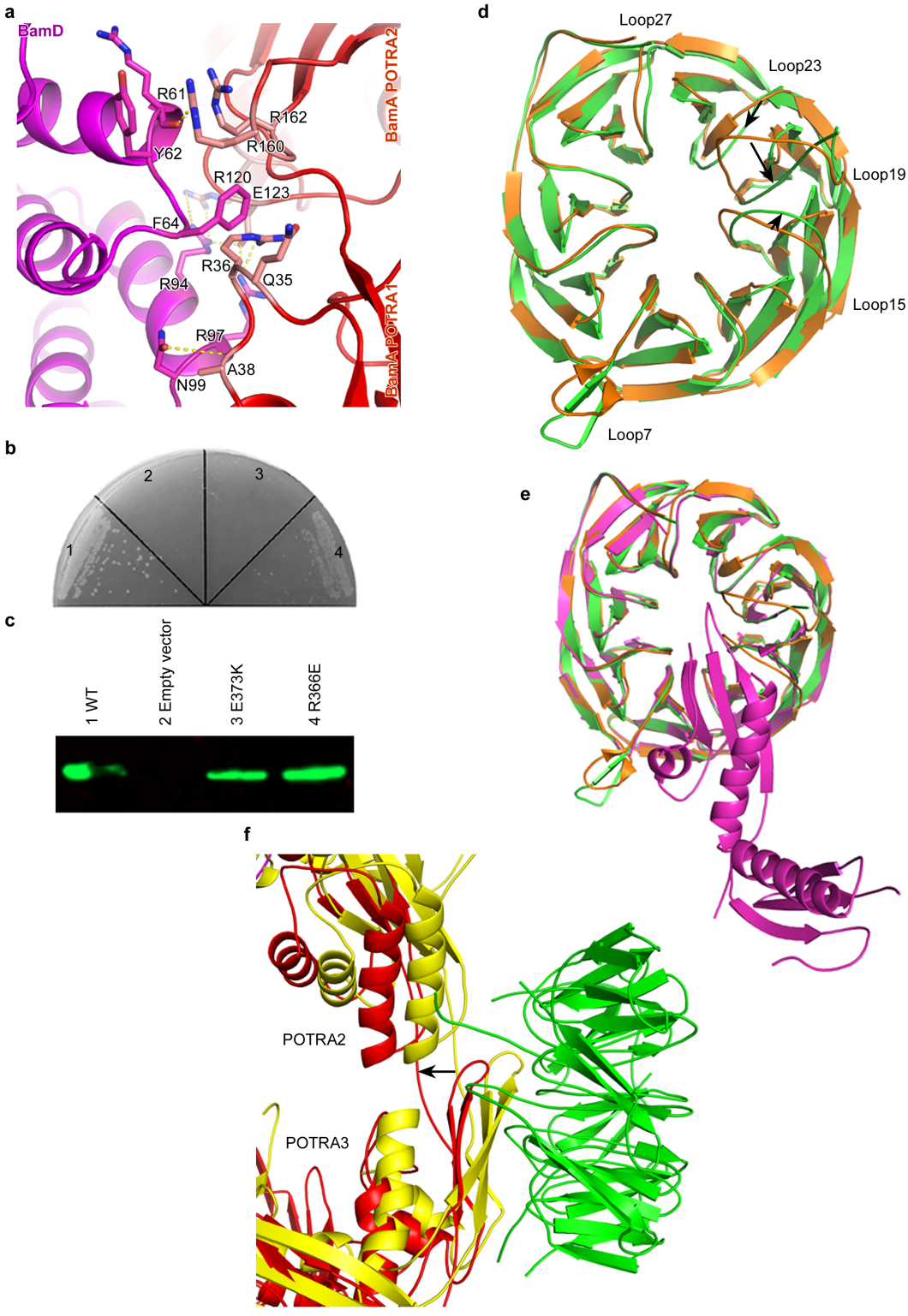

Extended Data Figure 7

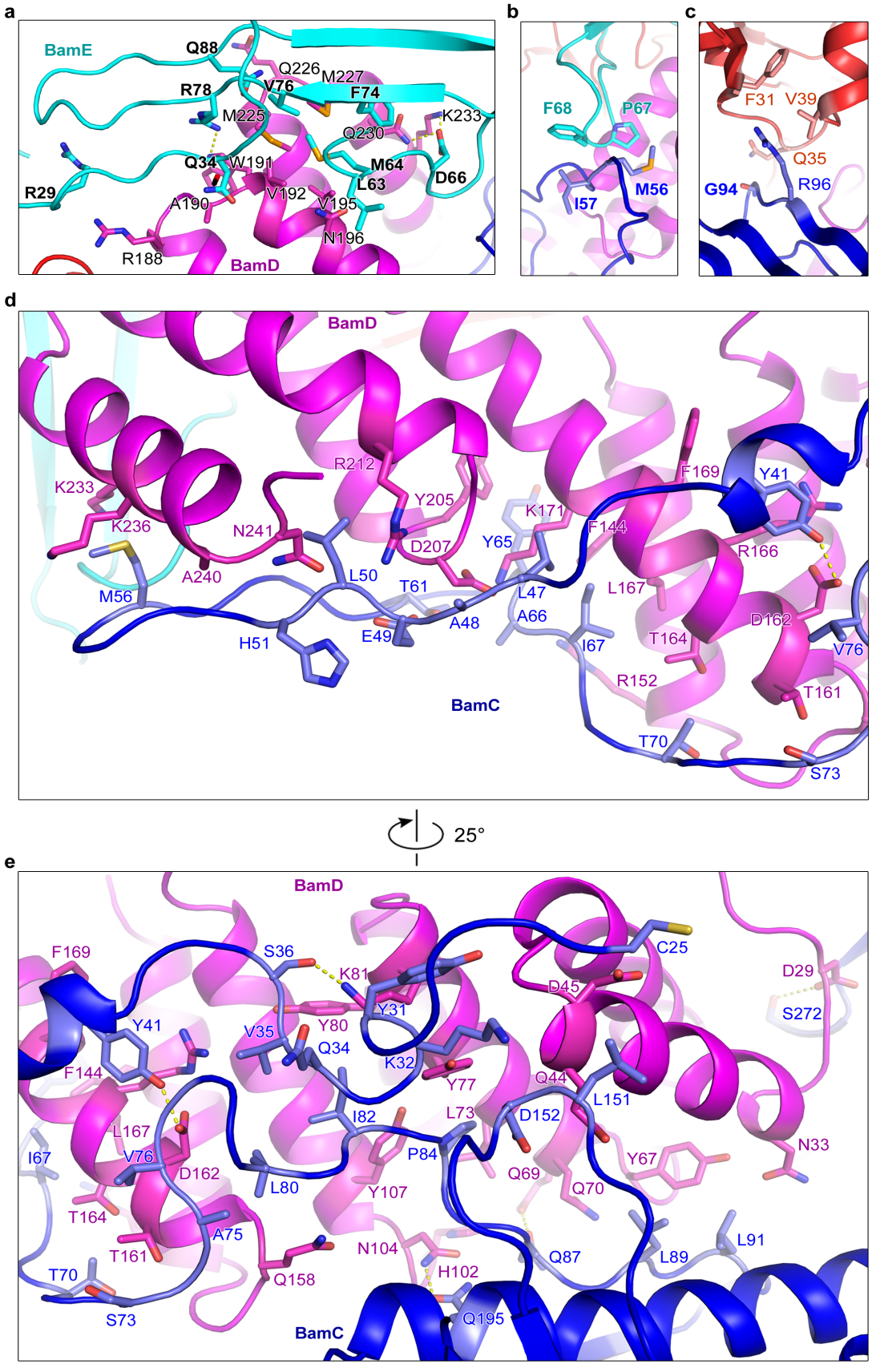

Extended Data Figure 8

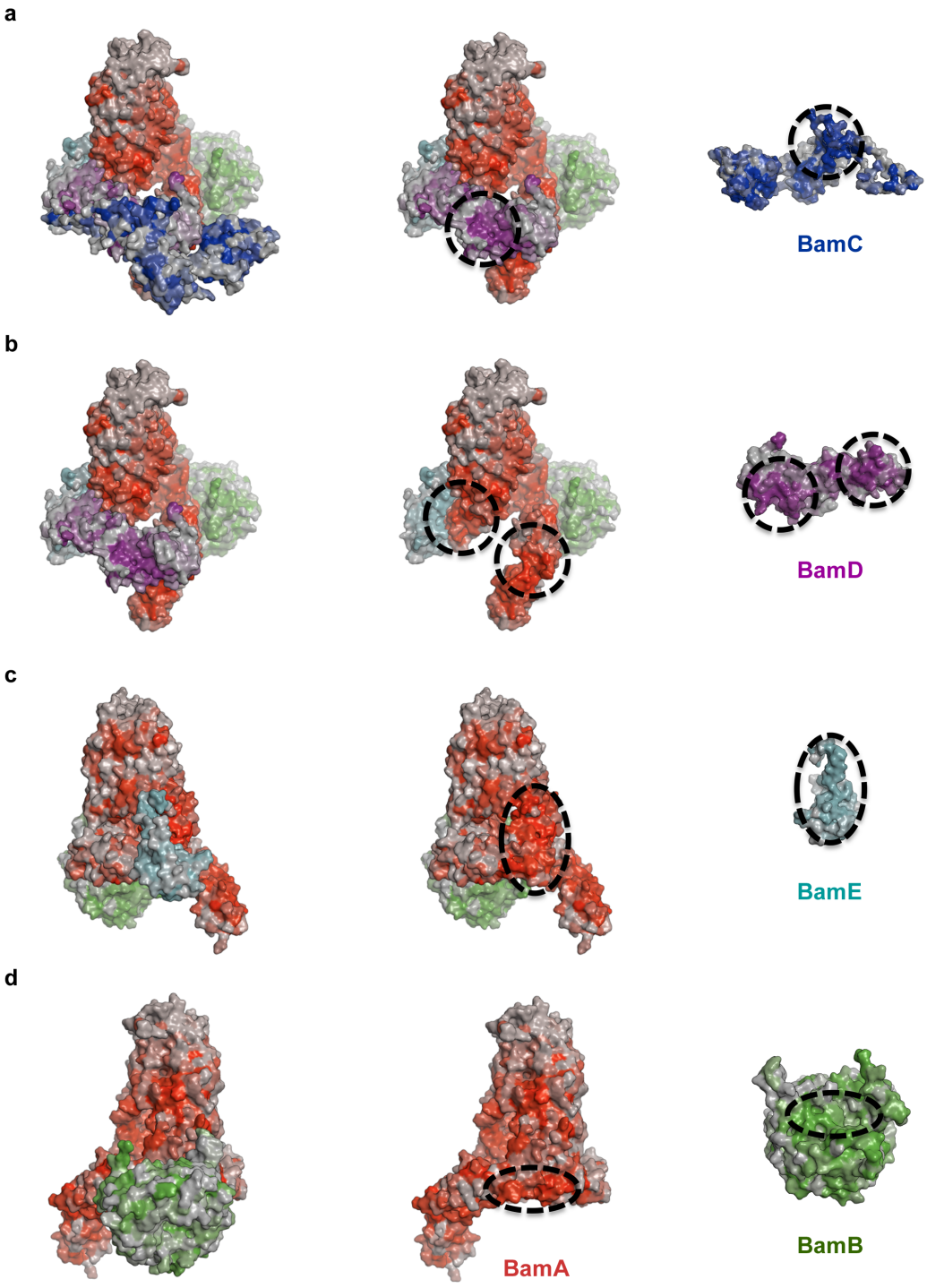

Extended Data Figure 9

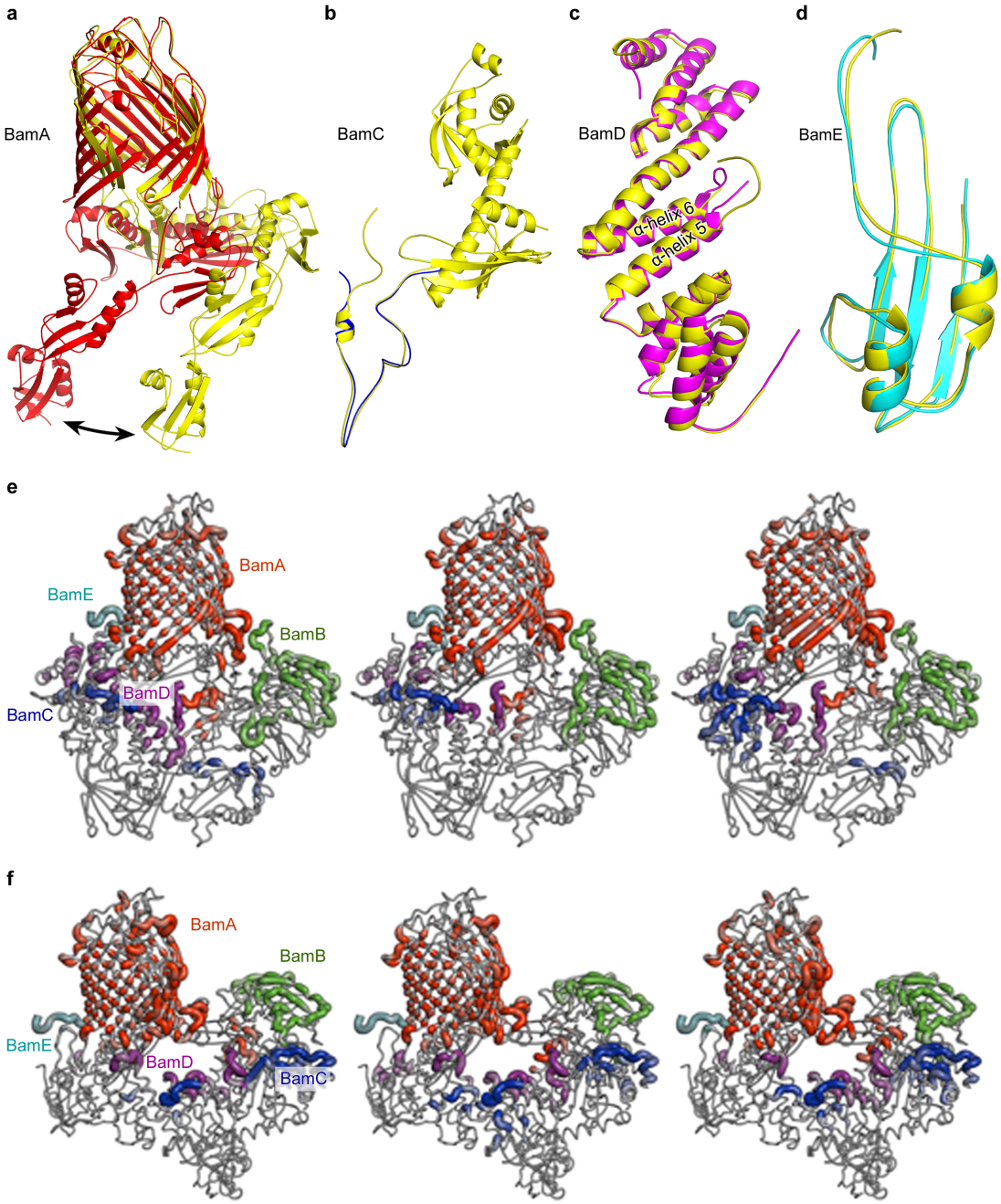

Extended Data Figure 10.

Extended Data Table 1 | Data collection and refinement statistics

	BamACDE Se-Met[‡a]	BamABCDE NaI[a]	BamABCDE Native[‡a]
Data collection			
Space group	$P4_22_12$	$P4_12_12$	$P4_12_12$
Cell dimensions			
a, *b*, *c* (Å)	254.16, 254.16, 179.22	116.72, 116.72, 432.44	116.69, 116.69, 435.19
α, β, γ (°)	90.0, 90.0, 90.0	90.0, 90.0, 90.0	90.0, 90.0, 90.0
Wavelength (Å)	0.97951	1.82330	0.97949
Resolution (Å)	29.94–3.90 (4.02–3.90)*	29.86–4.00 (4.27–4.00)	49.65–2.90 (2.97–2.90)
R_{merge} (%)	28.5 (>100.0)	24.8 (>100.0)	18.0 (>100)
CC1/2 (%)	99.9 (49.4)	100 (99.6)	99.8 (50.8)
$I / \sigma I$	11.0 (0.9)	37.0 (11.8)	15.0 (0.6)
Completeness (%)	99.8 (100.0)	98.5 (97.8)	100 (100)
Redundancy	27.1 (27.2)	158.00 (165.1)	26.4(23.8)
Refinement			
Resolution (Å)	29.92 – 3.90		49.65 – 2.90
No. reflections	73745		67553
R_{factor} / R_{free}	30.44/31.93		27.62/30.41
No. atoms			
Protein	19796		22815
Ligand/ion	0		0
Water	0		0
B-factors(Å^2)			
Protein	150		118
Ligand/ion	N/A		N/A
Water	N/A		N/A
R.m.s. deviations			
Bond lengths (Å)	0.010		0.009
Bond angles (°)	1.868		1.609
Residues in Ramachandran plot			
Favored (%)	90.5		91.6
Allowed (%)	8.7		7.7
Outliers (%)	0.8		0.7
PDB code	5D0Q		5D0O

*Values in parentheses are for highest-resolution shell.

‡ Highest resolution shell was taken as point where CC1/2 > 30 along strongest reciprocal lattice direction.

[a]Data statistics shown for each wavelength are a combination of two datasets (BamACDE Se-Met) and four datasets (BamABCDE NaI).

[b]$R_{factor} = \Sigma||Fo|-|Fc|| / \Sigma|Fo|$, where Fo and Fc are observed and calculated as structure factors, respectively.

[c]R_{free} is calculated using 5% of total reflections, which is randomly selected as a free group and not used in refinement.

Diffraction data for all structures were anisotropic and axis specific resolution cutoffs from AIMLESS (CC1/2>0.3) for refinement data basis are listed below for illustration:

BamACDE Se-Met h-k plane = 4.45 Å, l axis = 3.50 Å

BamABCDE Native h-k plane = 3.48 Å, l axis = 2.75 Å